Geballe Laboratory for Advanced Materials
McCullough Building
Stanford University
Stanford CA 94305

Final Technical Report

on

INVESTIGATION OF THE CRYSTAL GROWTH OF DIELECTRIC MATERIALS BY THE BRIDGMAN TECHNIQUE USING VIBRATIONAL CONTROL

For the Period

2/1/98-4/30/02

NASA Contract # NAG8-1457-06

Submitted to

National Aeronautics and Space Administration
George C. Marshall Space Flight Center
Marshall Space Flight Center, Al 35812

Robert S. Feigelson, Principal Investigator
Stanford University
Evgenii Zharikov, Co-Principal Investigator
General Physics Institute
Moscow, Russia

Submitted by
The Board of Trustees of
The Leland Stanford Jr. University
Stanford, California 94305

TABLE OF CONTENTS

1.0 Introduction

The principal goal of this ground-based program, which started on February 1, 1998 and concluded on April 30, 2002, was to investigate the influence of low frequency vibrations on the fluid flow and quality of dielectric oxide crystals grown by the vertical Bridgman method. This experimental program was a collaborative effort between Stanford University and the General Physics Institute of the Russian Academy of Sciences in Moscow, and included a strong emphasis on both physical modeling and the growth of some technologically important materials. Additionally it was carried out initially in collaboration with the theoretical and numerical investigations of A. Fedoseyev and I. Alexander (ongoing in another NASA sponsored program). This latter program involved a study of vibro-convective buoyancy-driven flows in cylindrical configurations with the expectation of being able to use vibrational flows to control buoyancy driven fluid transport to off-set the effect of "g-jitter" during microgravity Bridgman crystal growth. These two programs taken together, were designed to lead to a new parametric control variable which can be used to either suppress or control convection, and thereby heat and mass transport during Bridgman crystal growth. It was expected to be effective in either a terrestrial or space environment.

The experimental program was designed to verify and refine the results of the predictions made in the theoretical program, and lead to the design of vibration controlled growth systems which can be adapted to NASA flight ready crystal growth furnaces. It also was intended to provide recommendations for the use of this vibrational technology in space growth experiments.

The specific objectives of the program were as follows: 1) Investigate how applied low frequency vibrations affect fluid flow during Bridgman crystal growth and develop relationships between vibro-convective-mediated flows and crystal quality. This part of the program involved extensive experimental physical modeling using noncrystallizing water-glycerine mixtures and low temperature, transparent model growth systems. 2) Establish the most appropriate mode(s) for introducing low frequency vibrations into crystal growth systems with different physical and material properties, and optimize parameters for producing desirable fluid flow regimes (heat and mass transport conditions). Solve the specific technical problems associated with the introduction of vibrations into real growth systems. Design, and construct apparatus for fluid flow and crystal growth experiments, 3) Correlate vibration induced flows with a) interface shape and position, b) striations c) microsegregation, d) dopant distribution and e) crystal perfection , etc., 4) Demonstrate the effectiveness of vibroconvection control during the growth of nominally pure and doped technologically important dielectric oxide single crystals, 5) Verify and refine the theoretical predictions derived from mathematical modeling research, 6) Develop quantitative laws for predicting the most appropriate growth conditions for a specific material and system geometry and, 7) Provide recommendations for the use of vibrational technology in space and terrestrial growth experiments.

2.0 Background

It is well known that natural buoyancy-driven convection in terrestrial crystal growth systems can have a profound (often negative) influence on crystal quality (defects and homogeneity) and growth rates. As a result, various strategies have been employed over the last 50 years to either reduce these random, oscillatory flows (ex. the use of baffles, reduced thermal gradients, or a microgravity environment, etc.) or to introduce controlled flows via forced convection (ex. accelerated crucible rotation, seed rotation, ultrasonic vibrations, etc.).

A review of the literature reveals that very little research had been carried out to deliberately introduce low frequency (0-1000 Hz) controlled acoustic vibrations into crystal growth systems, and to systematically evaluate their influence on a wide range of physical, optical and electrical properties. This might be attributable to the fact that in most crystal growth situations mechanical disturbances were considered to be detrimental and are usually minimized. Several early papers [1-6] written in the 1960's, however, suggested that the application of vibrations to a growth system might be beneficial. In 1962 Langenecker and Frandsen [1], studied the influence of sonic and ultrasonic acoustic waves (100 to 25,000 Hz) on the growth of zinc crystals by the Czochralski method. They discovered that the critical shear stress increased by up to 80% over unvibrated crystals and attributed this to a rearrangement of dislocation networks. In 1967 Witt and Gatos [2] introduced 50 Hz vibrations into the Czochralski growth of Te doped InSb without disrupting single crystal growth. The authors suggested that this technique might provide "information regarding the incorporation of crystal defects, orientation defects and other aspects of the solidification process in general". In a third paper by Ikonnilova and Izergin [3], the application of 100 Hz vibrations (to the seed) during the Czochralski growth of KCl led to a 10-fold reduction in dislocation densities. The density was found to be a function of vibrational amplitude, decreasing with increasing energy until a minimum value was reached. Borshchevskii and Tretjakov [4] introduced 100 Hz vibrations into the crystallizing melts of a variety of semiconductors, including GaAs, CdTe and PbSe. The vibrations were introduced through the ampoule, and the most important result was that the authors obtained very large-grained and dense ingots and sometimes single crystals compared with nonvibrated melts. Nikitina et al [5] also applied 100 Hz vibrations to the Czochralski growth of Ge-Si and GaSb-InSb ingots. They reported enhanced homogeneity in their solid solution material. Krigintsev and Avvakumov [6] in a paper on melt stirring implied that acoustic vibrations might modify impurity distributions, reduce segregation, increase grain size and increase density. These results were at best tentative, however and the studies were not carried out in an extensive and thorough manner.

Several of the above results suggested that acoustic vibrations may have an effect on the diffusion boundary layer next to the growing interface, probably by a stirring phenomenon. Since the diffusion boundary layer is one of the fundamental limiting factors in all forms of crystal growth, the ability to reduce or modify it could be of profound importance.

The previously described research suggested that the introduction of vibrations into crystal growth systems can be divided into two convenient categories depending on whether

vibrations are applied externally or internally. An example of the former is when the vibrating body is placed on the growth ampoule or crucible (CVS method). In the latter case, the vibrating body is inserted directly into the melt or solution (AVC method).

2.1 Externally Applied Vibrations: The Coupled Vibrational Stirring Method (CVS)

Early in the 1980's, the Feigelson group at Stanford became interested in the eariler reports that low frequency vibrations could enhance grain size and reduce dislocation densities. This was an important problem in the Bridgman growth of CdTe single crystals. By applying 60 Hz vibrations along the growth axis they were successful in getting nearly single crystal boules of CdTe. In order to understand the relationship between these externally applied vibrations and the improved results, they did some preliminary modeling experiments on the influence of low frequency vibrations on fluid flow. They found that fluid flow was almost negligible when the vibrations were applied along the growth axis and that the mechanism for the improved results in CdTe growth must have been due to some other factor(s) [7]. On the other hand, they found that they could generate high rates of fluid flow in vertical Bridgman-like ampoules by applying two external orthogonal vibrators (of equal amplitude) normal to the growth axis (ampoule) [13]. This technique was named coupled vibrational stirring (CVS) and the results of this were first reported by Liu et al [13] in 1987.

In its most general form, CVS is an externally applied forced convection technique involving the coupling of two orthogonal vibrations in such a way that the vertical axis of the system is moved in the x-y plane with no rotation about the z-axis. In principle, the motion can be that of any elliptical figure depending on the frequency, amplitude, and phase angle selected for the vibrators. The simplest case, and the one used by the Feigelson group, is a circular path which can be acheived when the amplitudes and frequencies are the same. At operating conditions, the circular motion of the crucible produces a surface wave and mixing in the liquid (figure 1).

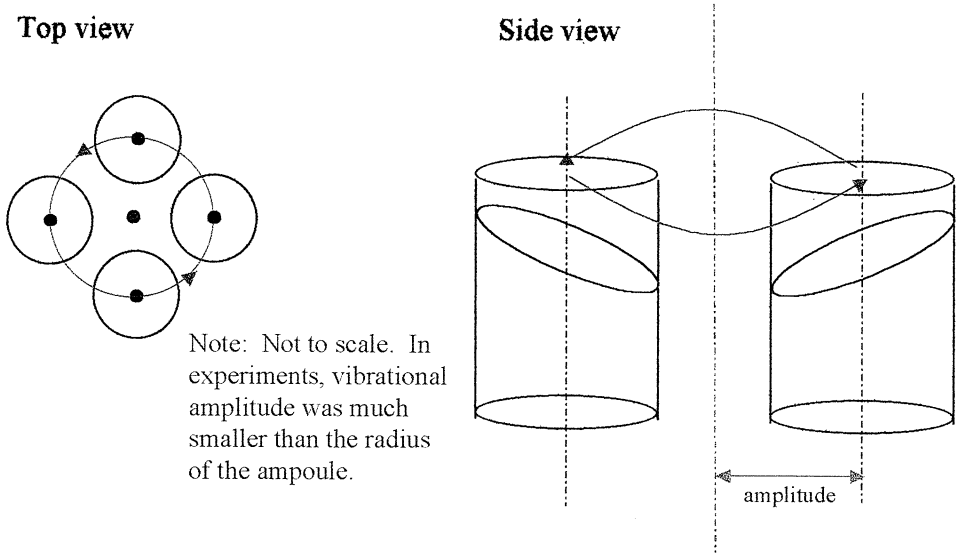

Figure 1. Schematic of CVS Motion

The intense CVS generated flows reported by Liu et al [13] were attributed to the surface wave created as the axis of the ampoule rotates in a circular orbit. Later work by Alexander [8] showed that vibrating an ampoule in a similar way but with the liquid surface capped will not generate fluid flow under isothermal conditions. The liquid in this case behaves as a solid.

Liu et al [13] performed preliminary experiments using CVS mixing on water/glycerin solutions. Complete system mixing was found to take only a matter of seconds. Figure 2 shows the typical mixing behavior observed (approimately one second elapsed between successive frames). Dye injected at the bottom can be seen moving up the middle in a spiral, while dye injected at the top moved down along the crucible walls. Mixing times and wave heights were observed as functions of several system parameters (such as vibrational frequency and fluid viscosity). In the $CsCdCl_3$ Bridgman melt system, the solid-liquid interface position was found to be a function of the vibrational frequency during CVS flows, demonstrating that CVS could be used to alter heat and mass transport in a melt system.

In 1990, Lu et al. [15] showed that CVS induced flows improved the homogeneity of Bridgman grown CdTe crystals, but with some degradation in crystalline quality as growth progressed. It was thought that the latter problem was due to the crystal rattling around in the ampoule during cooling.

DeMattei and Feigelson [16] examined the effects of CVS on temperature profiles in during the growth of $PbBr_2$. Application of CVS during growth flattened the temperature gradient in the melt. A thermal balance analysis of the growth interface region indicated that the temperature gradient at the interface was dramatically increased as a result of CVS flows. The increased interface gradient was expected to allow for higher growth rates without interface breakdown based on constitutional supercooling criterion.

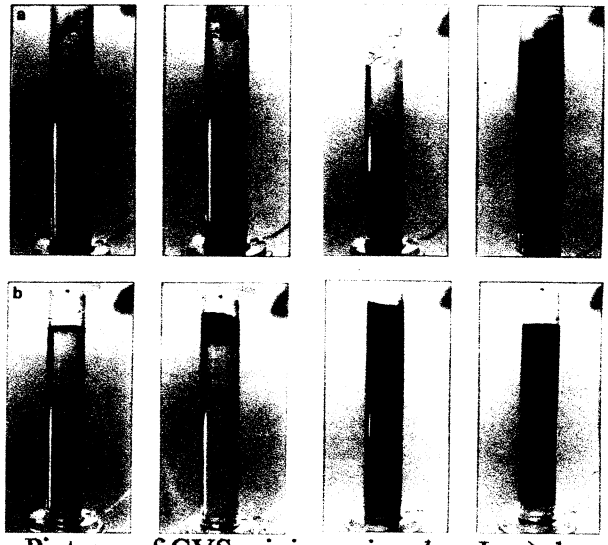

Figure 2. Pictures of CVS mixing using dye. In a) dye was injected at the bottom, b) at the top. [13]

The promising results from the previous studies of CVS on crystal growth prompted the further study of CVS in this report.

2.2 Internally Applied Vibrations: The Axial Vibrational Control Method (AVC)

Around the same time that the Feigelson group was beginning to examine the effects of CVS on Bridgman systems, E.V. Zharikov et al. were investigating the effects of introducing low-frequency vibrations into Czochralski melts [17]. Vibrations were applied axially (along the growth direction) through the seed rod at the surface of the liquid. Vibrational flows were studied in sodium nitrate melts with the aid of aluminum tracer particles. They found that vortex flows were generated near the growing crystal. They related the form, dimension, and intensity of the flows to the vibrational parameters and liquid properties, and analyzed the effects of vibrational convection on heat and mass transfer during crystal growth.

Further work by Zharikov et al. [18] studied temperature fluctuations in the melt that were brought about by this convection technique. They also used this technique to grow YSGG crystals [19]. The vibrations were found to have a substantial effect on interface shape and microscopic homogeneity.

Zharikov and coworkers' experiments with vibrations on Czochralski melt surfaces led to the idea of completely submeging the vibrating body in the melt. This submerged vibrator technique was named axial vibrational control (AVC).

AVC is an internally applied forced convection technique involving the the vibration of a body completely submerged in the melt. Vibrations are applied axially (along the growth direction) in order to produce fluid flow, and the vibrating body can be of any shape.

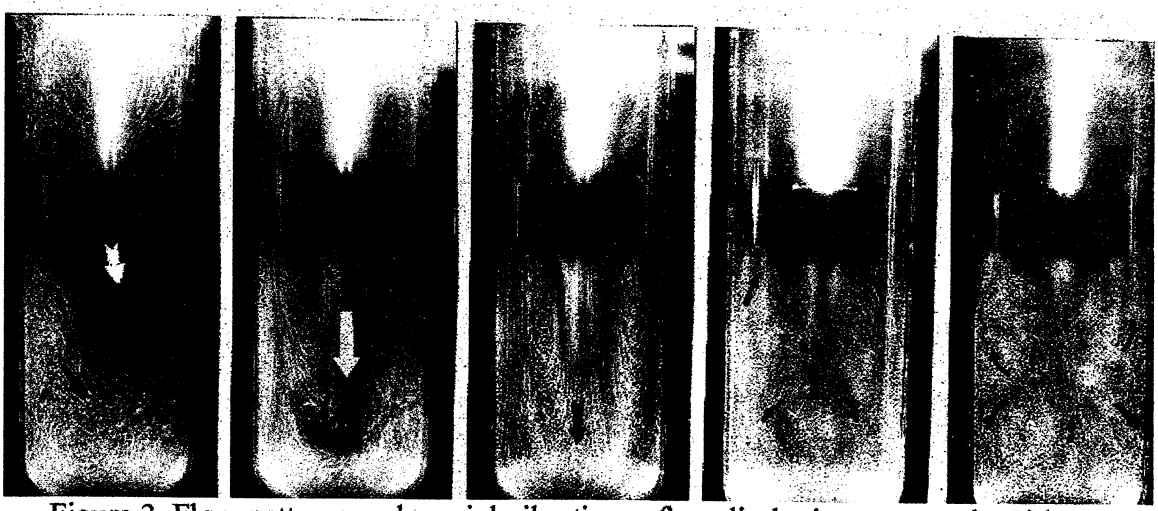

Figure 3. Flow patterns under axial vibrations of a cylinder in an ampoule with diameter of 41 mm. Settings for pictures from left to right: a) f=80Hz a=50μm b) f=80Hz a=100μm c) f=80Hz a=200μm d) f=80Hz a=300μm e) f=80Hz a=500μm

In 1997, Zharikov and coworkers [12] looked at the influence of a submerged vibrating body on fluid flow. They found that strong controlled forced convection could be induced, and studied the flow patterns and stability as a function of the amplitude-frequency parameters of the body. Several different vibrator configurations were studied including spheres, cubes and cylinders (the latter with various shaped bottom faces). The case of a vibrating cylinder or disk produced vortices with cylindrical symmetry and was convenient to use in cylindrically shaped crucibles. Flow patterns produced through this technique are shown in figure 3. The submerged disk version of AVC, applied to Bridgman growth in cylindrical crucibles, was studied in this report.

2.3 Summary

Both the CVS and AVC methods can generate strong flows and therefore substantial fluid mixing, and will affect heat and mass transport. The flow patterns, however, are quite different, and each method has a set of advantages and disadvantages. For example, the CVS method can be used with a completely sealed system quite easily. This is important for volatile systems or those which react with the ambient atmosphere. However, studying CVS flows is very difficult because the entire crucible as well as the fluid are in out-of-plane motion. In the AVC method, the choice of material for the vibrator is important as it is directly placed into the melt, and it is difficult to work in a sealed system. Visualization and analysis of flows in the AVC system is easier than with CVS because the crucible is stationary.

3.0 Experimental Procedure

3.1 Fluid Flow Modeling

Two model fluids were used in this report in order to study vibroconvective flows. Water/ glycerin solutions were used in order to study a wide range of operating parameters at room temperature. Sodium nitrate was used as a model low-temperature melt system. Some of the basic thermophysical properties for these liquids are listed in table 1 below.

Table 1. Thermophysical properties of model fluids [20]

Property	Water (t = 30^{O}C)	$NaNO_3$ (t = 310^{O}C)
Melting point, ^{O}C	**0.0**	**307.0**
Liquid density, g*cm^{-3}	**0.996**	**1.889**
Dynamic viscosity, g*cm^{-1}*s^{-1}	**8.01×10^{-3}**	**2.78×10^{-2}**
Kinematic viscosity, cm^2*s^{-1}	**8.0410^{-3}**	**1.4710^{-2}**
Thermal diffusivity cm^2*s^{-1}	**1.48×10^{-3}**	**1.58×10^{-3}**
Coefficient of volumetric expansion, K^{-1}	**2.8×10^{-4}**	**6.6×10^{-4}**
Prandtl number	**5.4**	**9.3**

3.2 CVS Setup

The CVS drive mechanism used in these experiments is shown in figure 4. It consisted of a motor attached to the crucible via an offset pin. A y-shaped sliding plate between two stationary plates forms an air bearing for the system that is used to ensure that the system is level and that no wobbling or tilt occurs. Two basic parameters, vibrational amplitude and frequency, were adjusted to give the desired flow behavior. Vibrational amplitude was adjusted by changing the displacement of the shaft connector located between the motor and the crucible. Shafts with displacements of 0.8, 1.6, and 2.3 mm were available. An amplitude of 1.6 mm was used for most experiments. Vibrational frequency was adjusted by changing the motor speed. Frequency adjustments were technically much easier as they only required adjusting a 10 turn potientiometer, while amplitude adjustments required physically altering the setup.

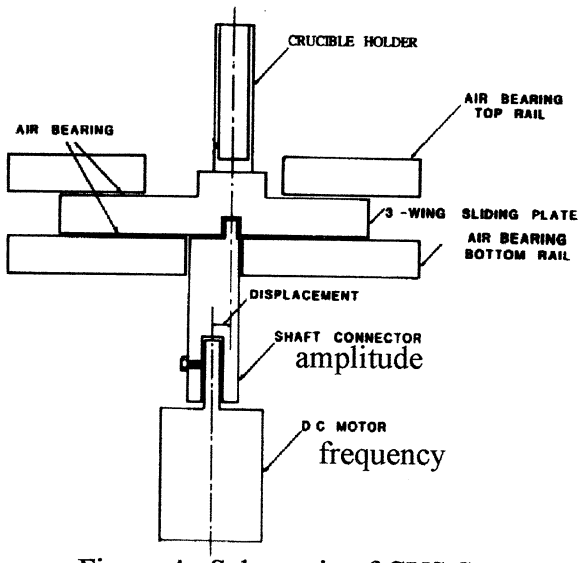

Figure 4. Schematic of CVS Setup

3.2.1 Water/Glycerin System

The water/glycerin system was used to study the importance of ampoule geometry, vibrational parameters, and fluid viscosity on CVS generated flows. All of the ampoules under study were of cylindrical shape and were made from acrylic plastic. Ampoule geometry was varied by changing the diameter of the cylinder from 2.2 to 7.0 cm and by changing the height of the liquid in the ampoule. Fluid viscosity was altered by mixing different ratios of water and glycerin from 1.0 to 10.0 cp.

Three general types of experiments were performed using this system: dye experiments, wave height experiments, and tracer particle experiments. Dye experiments were used to obtain qualitative flow patterns and to measure mixing times. Wave height experiments were used to examine the effects of vibrational parameters on the surface wave produced by the system and the effect of the surface wave on flow. Tracer particle experiments were used to gain a more quantitative picture of the flow patterens and flow velocities during CVS motion through the use of streak photography and video.

In dye experiments, powdered RIT^{TM} blue dye was mixed with the appropriate viscosity solution and injected into the bottom of the ampoule using a syringe and a small diameter teflon tube. Mixing times were measured with the use of a focused red LED and a photodetector. The LED and the detector were attached to the ampoule on opposite sides and placed at 2/3 height from the bottom of the liquid (figure 5). Photodetector output was measured with a strip chart recorder. Typical optical transmission, as measured by the photodetector, decreased as the dye began mixing and reached a steady value when the dye was homogeneously mixed (figure 6).

In particle experiments, neutrally buoyant particles (Pliolite VTL^{TM} manufactured by Goodyear Chemical Co.) with densities of 1.01 g/cm^3 and a particle size distribution in the range of 10-100μm were used. Particles were illuminated using a low power laser (red laser pointer) passed through a cylindrical lens to form a plane of light or 'light sheet.' A

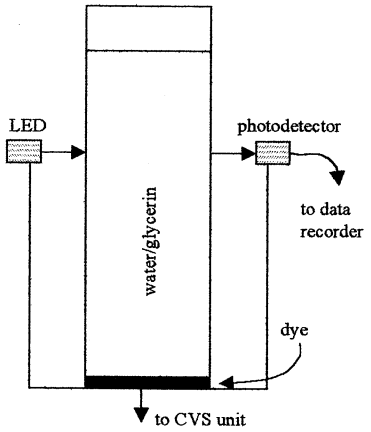

Figure 5. Mixing Time Setup

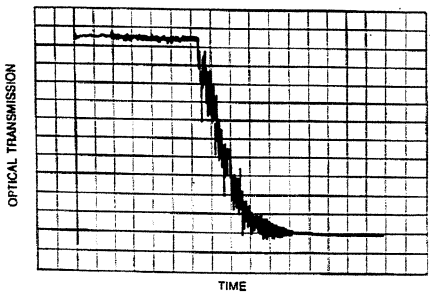

Figure 6. Typical Photo Detector Output

covering made from foam-core board was placed around the CVS setup in order to block extraneous light. Images were recorded using either a still camera with adjustable shutter speed or a video camera. Figure 7 shows a typical CVS setup for the particle experiments, and figure 8 shows a schematic of lighting for particle observation.

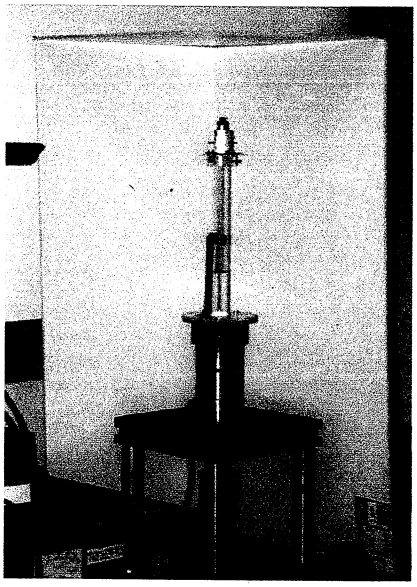

Figure 7. Photo of water/glycerin setup - set for particle experiment

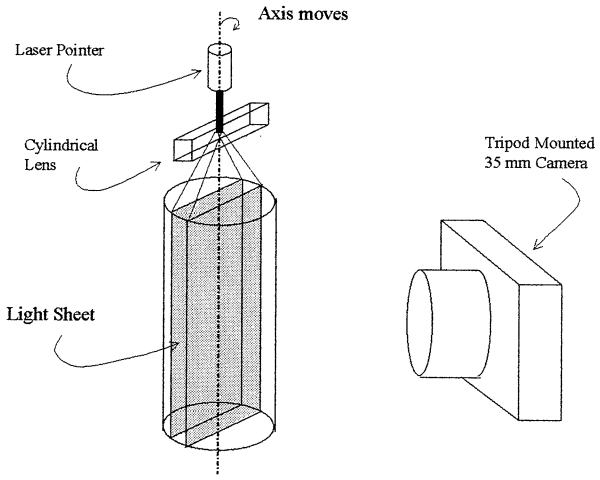

Figure 8. Lighting and camera setup for particle experiments

3.2.2 Low Temperature Melt System: $NaNO_3$

Sodium nitrate was chosen as the low melt temperature, model oxide material because both the crystal and the melt are transparent and many important fluid flow parameters have been determined for this melt system [9] some of which are given in table 1. The low temperature system was used to directly examine the effect of induced flows on the inter-

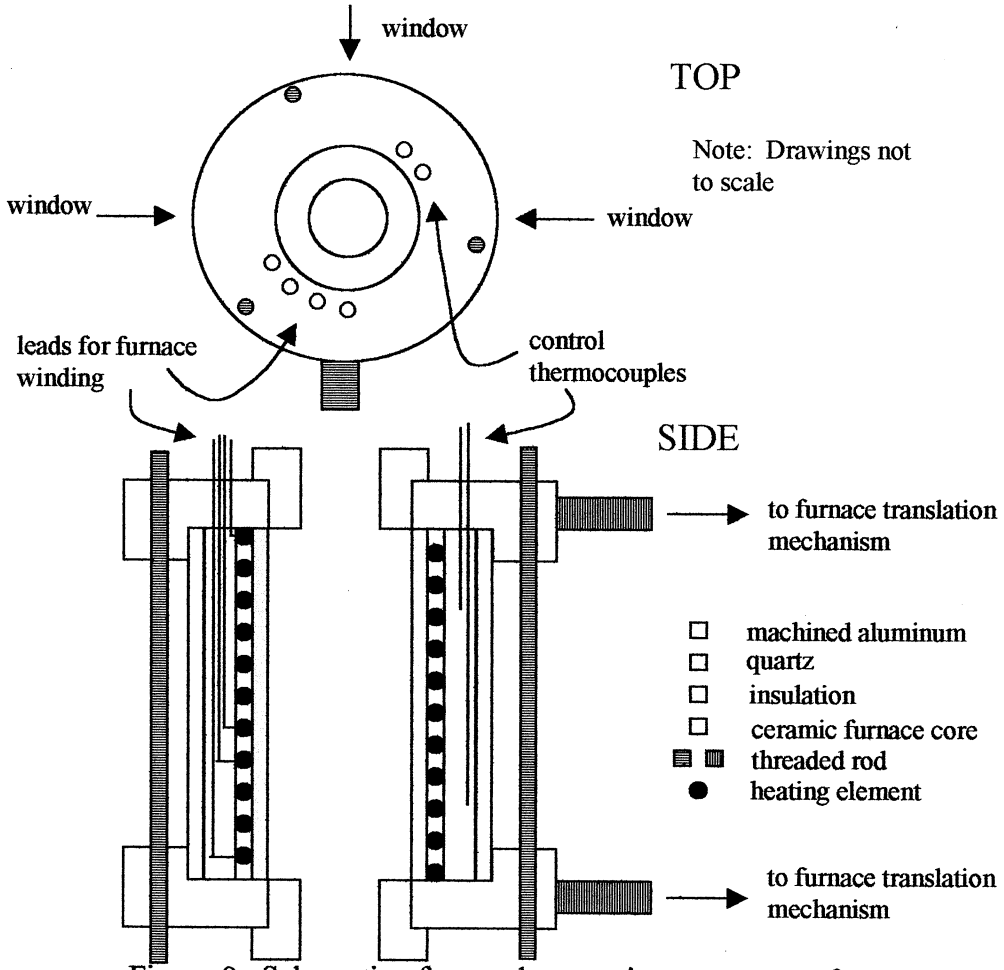

Figure 9. Schematic of second generation transparent furnace

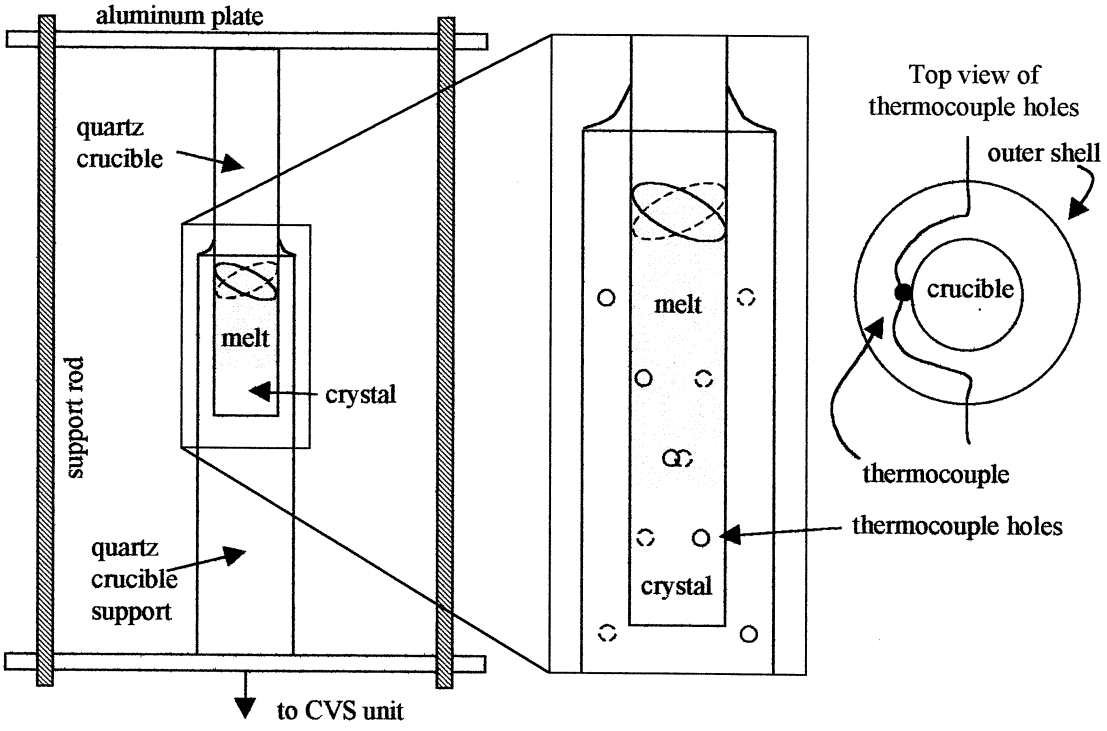

Figure 10. Schematic of quartz crucibles and holder

face shape and position, growth rate, interface stability, and temperature gradients in growth and non-growth conditions.

In order to directly observe the effect of CVS on the crystal growth system, a transparent furnace was fabricated. The furnace contained two independent zones made from Kanthal wire and two quartz windows for observation and back lighting. The furnace was 20 cm long and had a 3.8 cm bore. A second generation transparent furnace was later fabricated that improved upon the first design by 1) increasing the bore diameter to give more clearance to the moving crucible during CVS and 2) adding an extra observation window to allow for side lighting. A schematic of the second generation furnace can be found in figure 9. Its dimensions were 25.5 cm in length with a 6.5 cm bore. The bore was partially filled with insulation as indicated in the schematic. The insulation minimizes air convection in the furnace and can be easily replaced to accomodate crucibles of different diameters. Unless otherwise noted, $NaNO_3$ experiments were performed in the second generation furnace.

Flat bottom, cylindrical quartz crucibles with an inside diameter of 1.8 cm were used. A schematic of the crucible and holder can be seen in figure 10. A quartz tube was welded around the crucible and used to support and position the crucible in the furnace. Ten, 1 mm holes for thermocouples were placed in the spacer section of the quartz in such a way that the thermocouples would touch the outside of the crucible. The upper and lower part of the crucible was held in place by clamping it between two aluminum plates using three support rods spaced 120° from each other. The holder was designed so that during use, the crucible was inside the furnace and the support rods were outside of the furnace housing.

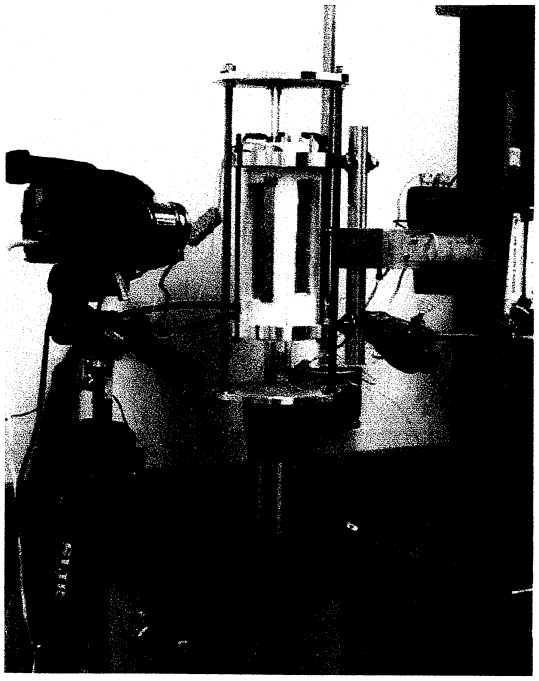

Figure 11. Photo of $NaNO_3$ setup

The setup for a typical $NaNO_3$ experiment can be seen in figure 11. The furnace was moved vertically via a puller arm (shown on the right of the picture). Furnace translation was the driving force for unidirectional solidification. The CVS unit was attached to the bottom of the crucible holder, so that only the crucible and holder were affected by the circular CVS motion. Upon assembling, the alignment and leveling of the system was critical so that the furnace and crucible did not touch each other.

Images of the $NaNO_3$ experiments were recorded using either a black and white CCD camera or a color video camcorder. The camera was routed to a VCR and a monitor so that images

could be recorded and viewed simultaneously. The best lighting for both cameras was found to be side lighting provided by a focused incandescent light (seen in figure 11). Alternate lighting using the 'light sheet' descibed earlier was used on occasion.

3.2.3 High Temerature System: $(1-x)PbMg_{1/3}Nb_{2/3}O_3 - xPbTiO_3$

One of the original goals of our program was to apply the knowledge gained through the modelling experiments to improve the growth of a technologically important dielectric oxide material. Results from the previously described model experiments were used to design an experiment using the lead magnesium niobate-lead titanate (PMNT) growth system. The PMNT system has been of recent technological interest due to its reported ultra-high strain and piezoelectric properties [10]. This particular system was chosen because of our recent experience in growing these crystals using the vertical Bridgman technique. Large compositional variations in the boules along the growth direction have been a problem. It was hoped that the compositional uniformity could be improved by using CVS to counteract buoyancy driven convection generated by radial thermal gradients.

PMNT was grown using a high-temperature Bridgman furnace with eight $MoSi_2$ heating elements (figure 12). The crucible was translated through a stationary furnace in order to induce growth. Due to the high melting temperature (~1300°C) and the high vapor pressure of lead oxide, a sealed Pt crucible was used. In this experiment, the cylindrical crucible had a flat bottom, straight-walls, and was fabricated from 0.20 mm Pt sheet. The crucible was double walled in order to minimize leaking effects which had been previously observed in the PMNT/Pt system. The inside diameter was 1.8 cm, identical to the $NaNO_3$ experiments. The length was 15 cm.

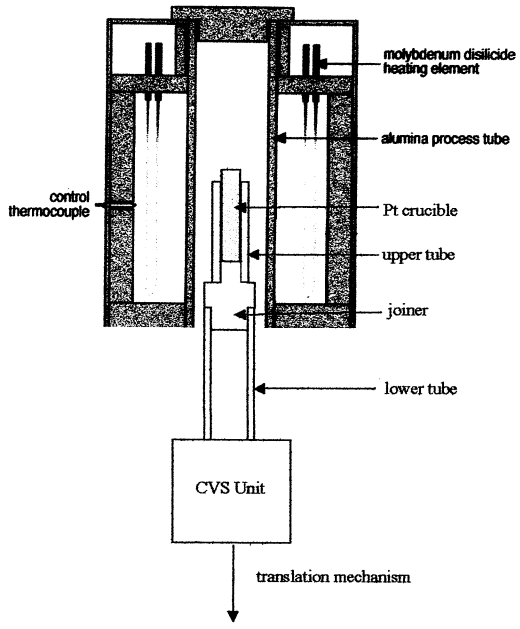

Figure 12. Schematic of PMNT setup

Mounting the crucible on the CVS apparatus was accomplished using two alumina tubes and a castable ceramic joiner. The lower piece of tubing was chosen to fit tightly into the CVS mount to prevent wobbling. It had an outside diameter of 3.4 cm. The upper tube had an inside diameter of 1.9 cm and was chosen in order to fit the Pt crucible exactly. The joiner was made from Zircoa castable ceramic 8D and was reinforced with five, thin (~3 mm dia) alumina tubes. This composite was chosen to join the two tubes precisely and remain structurally stable under high temperature and vibration conditions.

In order to monitor temperature, holes for thermocouples were drilled into the alumina tube containing the crucible as

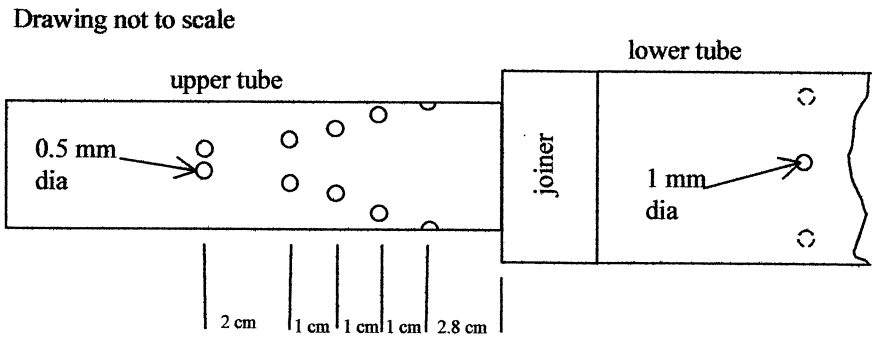

Figure 13. Schematic of the thermocouple hole pattern

shown in figure 13. Pt/PtRh thermocouples were inserted into the 0.5 mm dia. holes and pressed against the inside of the alumina tube in order to allow the Pt crucible to fit. The bottom thermocouple was not bent around the inside of the tube but instead rested on the top of the joiner. The thermocouple wires ran down the outside of the support tubes with the portion inside the furnace sheathed in thin alumina casings and the portion outside of the furnace sheathed in teflon. The alumina sheathing was tied securely to the alumina tubing using Pt wire.

Due to the positioning of the CVS apparatus under the furnace, the crucible and support tubes could not be loaded from the bottom. In order to lower the crucible and support tubes through the furnace and into the CVS mount, wires were placed into three 1 mm dia. holes that were drilled into the lower alumina tube.

Growth was seeded using a PMNT crystal previously grown in our lab during the spring of 2000. A <111> oriented, cylindrical seed of 2 cm in length was cut and ground from this crystal. The powdered PMNT charge contained 32%PT. It was produced by the columbite precursor method [11] and filled the remainder of the sealed crucible.

3.3 AVC Setup

Internal vibrations were implemented using a technique called axial vibrational control (AVC). In this technique, vibrations are introduced by submerging a body into the fluid and vibrating it along the growth axis. A schematic of the configuration used in this study can be found in figure 14. In this scheme, the vibrator was a submerged disk.

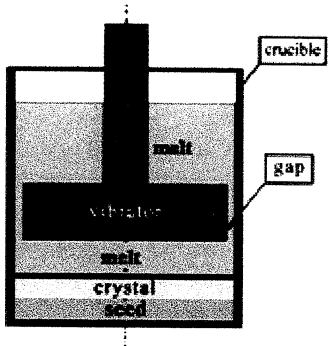

Figure 14. General schematic of the AVC setup

The submerged body must be able to withstand both chemical attack and the temperatures encountered. Unless otherwise stated, the AVC systems used in this study was made from quartz. These did not react with melts used and can withstand the melting temperatures.

3.3.1 Water/Glycerin System and Math Modelling

Some studies of the water/glycerin AVC system had been reported before the funding period of this project [12]. Further studies were conducted in both terrestrial and micro-gravity environments to expand upon this work. Experiments that were performed over this funding period included a microgravity experiment flown on the Russian Mir space station and terrestrial experiments to compliment the space experiment. Mathematical modelling of the water/glycerin system and melt systems were used to predict and explain fluid flow behaviour.

The earth and space experiments were conducted in a special vessel (figure 15) that was similar to the crucible used for the Bridgman growth of crystals. The vessel consisted of a cylindrical ampoule (6), manufactured from a plexiglas with a bore diameter of 26 mm and a height of 30 mm. The internal and external surface of the ampoule were optically polished. Oscillations were carried out using a rod (4) attached to the vibrating disk (5) through an elastic diapraghm (3) that hermatically sealed the ampoule. Vibrations were created with acoustic power (1) operating at 0.5 W.

The experiments were conducted with two transparent model fluids, one, a water/glycerin mixture and the other, silicone oil. Aluminum particles of 20 μm size were added to the fluids to visualize flows.

Mathematical modeling was performed on the basis of the direct solution of the axisymmetrical unsteady Navier-Stokes-Boussinesq problem. We studied the influence of vibrations on the boundary layers in Bridgman crystal growth and on heat and mass transfer during crystal growth in ground-based and microgravity environments.

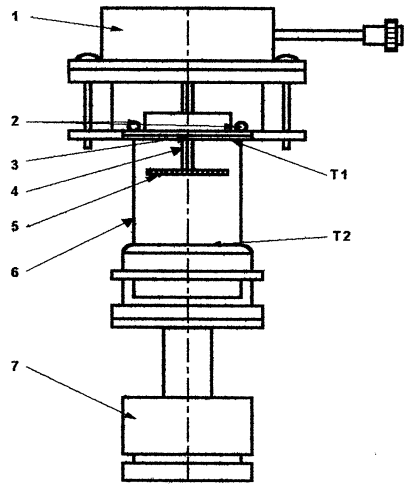

Figure 15. Schematic of space experiment equipment: 1) vibrator, 2) input channels, 3)diaphragm, 4) rod, 5) vibrator disk, 6) ampoule, 7) heater

3.3.2 Low Temperature Melt System: $NaNO_3$

Sodium nitrate was used for the same reasons as described in section 3.1.2. This low temperature system was used to examine the influence of vibrations on growth interface shape, crystal quality (dislocation densities), and dopant segregation.

In order to directly observe the effect of AVC on the crystal growth system, a transparent furnace was fabricated. A schematic for the system can be found in figure 16 and a picture of the system in figure 17. The major sub-systems involved in the low temperature AVC apparatus include: 1) the growth furnace, 2) the power supply system, 3) translation systems for the growth ampoule and vibrator, 4) computer-based control unit, and 5) the visualization sub-system.

The seven-zone transparent quartz furnace was resistively heated. The furnace heaters, translation mechanisms and vibrator were controlled via a personal computer and CAMAC crate. Temperature profiles in the 7-zone furnace were controlled to an accuracy of 0.3 K. A constant distance was maintained between the vibrating disk and the growth interface during experiments through the use of a translator mechanism seperate from that used to move the furnace. Two step-servo motors working in the speed range from 0 up to 300 mm/h were used for movement. The total translation length for the ampoule was 130 mm and for the vibrator, 50 mm.

The growth was conducted in quartz ampoules with inside diameters of 13 mm. Vibrations were introduced through the use of an electromagnetic transducer controlled by a PC sound card with low-noise amplifier generated low-frequency (LF) oscillations in the range of 20 - 100 Hz. . The oscillating body used in these experiments was a quartz disk (d=11 mm) submerged into the melt and attached to the vibration mechanism through a quartz rod.

Melt tracers made from corundum particles in the size range of 10-15 μm were used to visualize flows. Lighting was provided by a 5 mW red laser diode (650 nm) passed through a parabolic lens forming a "light knife". An analog videocamcorder in conjuction with a digitizing interface MiroVIDEO DC-30 and original software were used to characterize the interface shape and analyze flow patterns. The signal from the camcoder was transferred to the PC allowing for the digitization of the most characteristic moments of the growth process.

3.3.3 High Temperature Systems: TeO_2 and PbTe

Paratellurite (TeO_2) and lead telluride (PbTe) were chosen as high temperature materials for study using the AVC system. Two generations of furnaces with atmosphere control were designed and fabricated for the growth of these high-temperature materials. The first generation furnace was primarily used in the growth of paratellurite, and the second generation improved upon problems in the first and was used to grow lead telluride.

A schematic of the first generation furnace can be found in figure 18. The furnace had seven independent heating zones and could operate up to 1000°C. Furnace dimensions

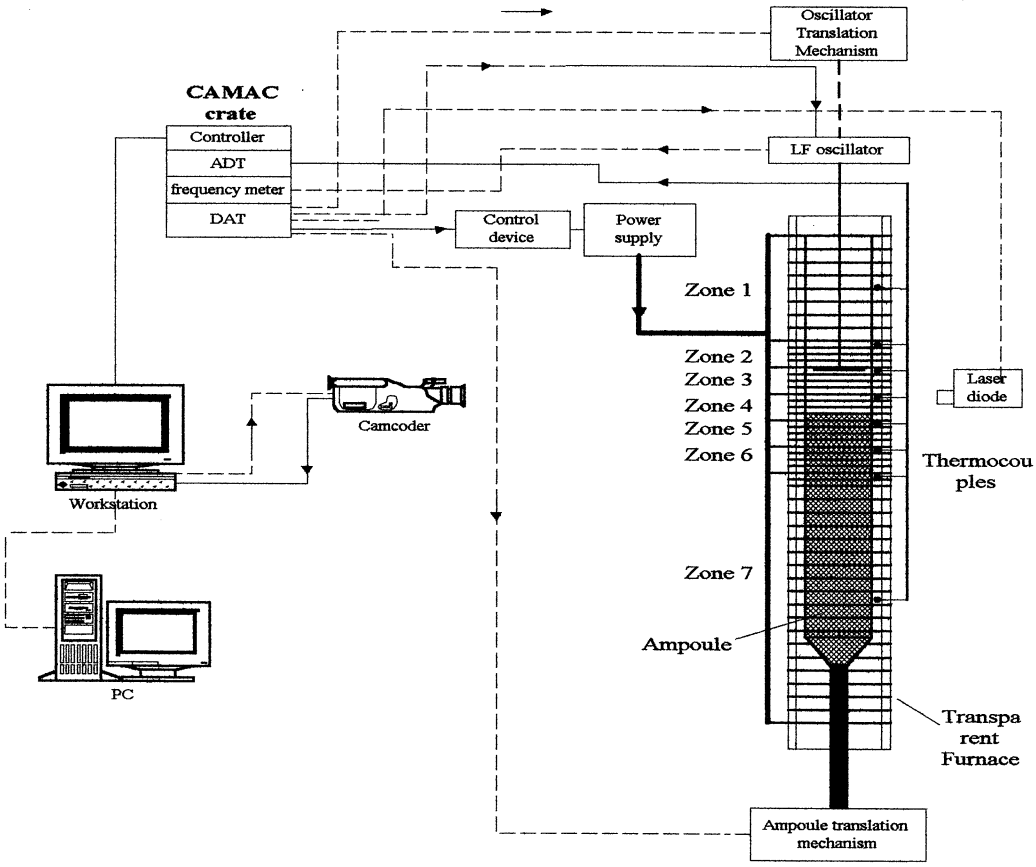

Figure 16. Schematic of low temperature AVC setup

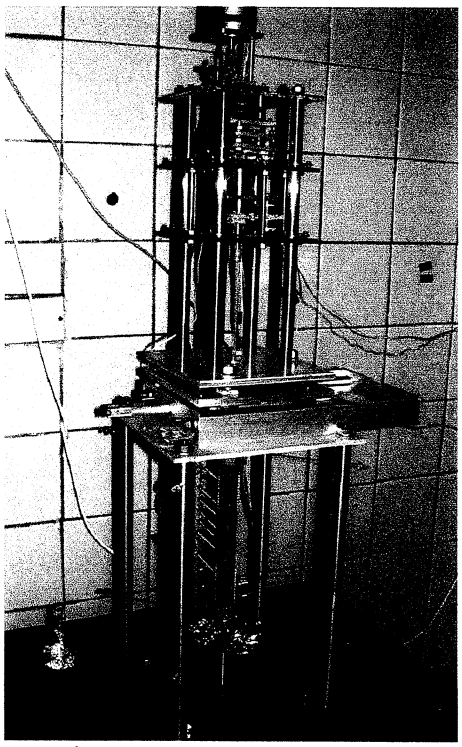

Figure 17. Picture of low temperature AVC system

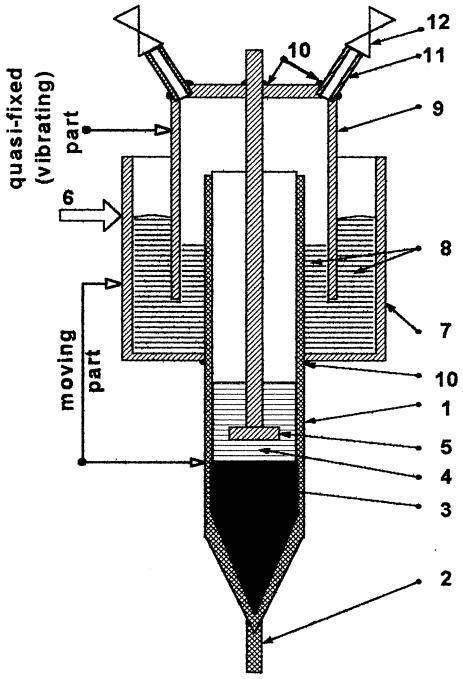

Figure 18. Schematic of first generation (paratellurite) system

allowed for the growth of crystals up to 18 mm diameter and 100 mm long. The parts of the furnace labeled 1-12 in figure 16 are as follows: 1) quartz ampoule, 2) quartz holder, 3) crystal, 4) melt, 5) quartz disk, 6) melt level control, 7) extrenal wall hydroseal, 8) Ga-In eutectic (or Ga) melt, 9) vibrating wall hydroseal, 10) welding spots, 11) outlets for atmosphere control, 12) gas seal.

The gas-controlled growth reactor shown in figure 18 consists of two major systems: the moving part and a quasi-fixed (vibrating) part. The moving part contains the growing crystal and moves through the furnace during the growth process. The vibrating part is stationary relative to the furnace, thus keeping the vibrating disk at a constant distance from the growth interface. The Ga-melt level in the hydroseal changes and the inert gas in the ampoule heats during growth. The pressure increase due to the heated gas causes another change in the Ga-melt level. The amplitude-frequency parameters in the reactor also can change. With the vibrational frequency fixed at a constant value, we had to continuously monitor and correct the vibration amplitude as well as the gas pressure in the reactor. An induction detector was designed and fabricated to allow measurement of the vibrational amplitude within 10 μm accuracy in the 10-100 Hz range. The Ga-melt level was also monitored to prevent hydroseal drainage. The Ga-melt level and gas pressure were manually controlled.

The second generation furnace attempted to correct the following problems caused by the design of the first generation furnace: 1) the amplitude-frequency control and continuously changing Ga-levels produced a very complicated system to control, 2) the gas atmosphere was limited to gases that would not react with the melt or the hydroseal liquid, 3) quartz was the only material that could be used for an ampoule in this system, 4) gas pressures were limited to a range of 760 +/- 100 torr in the reactor.

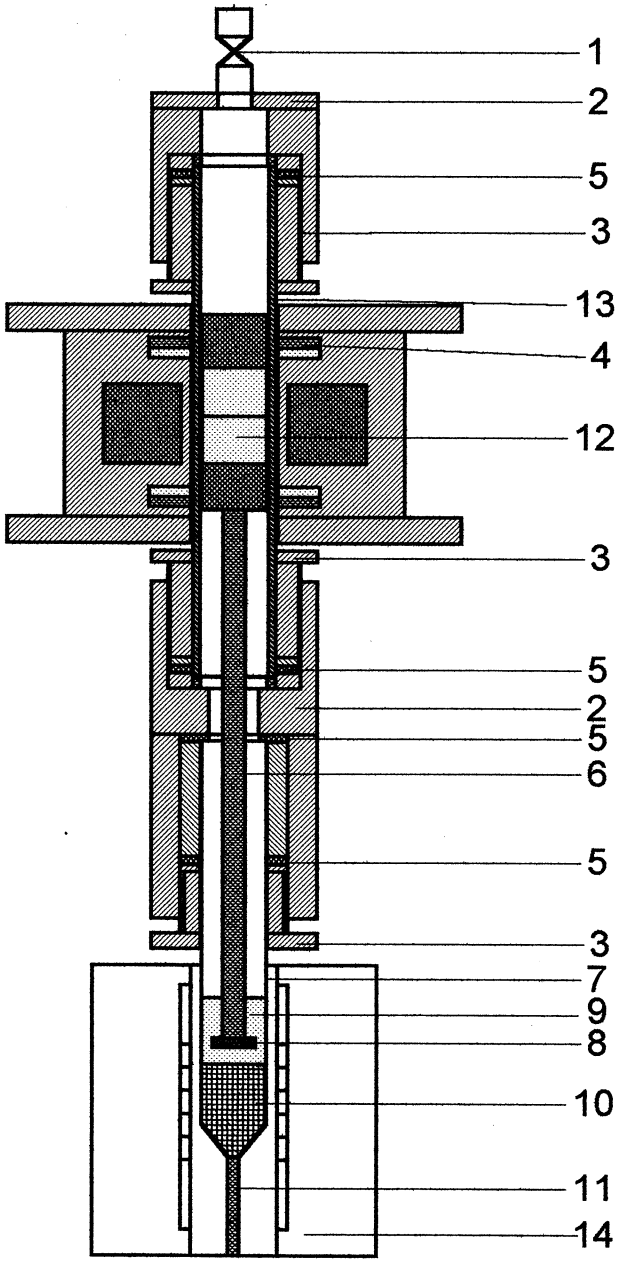

Figure 19. Schematic of PbTe system

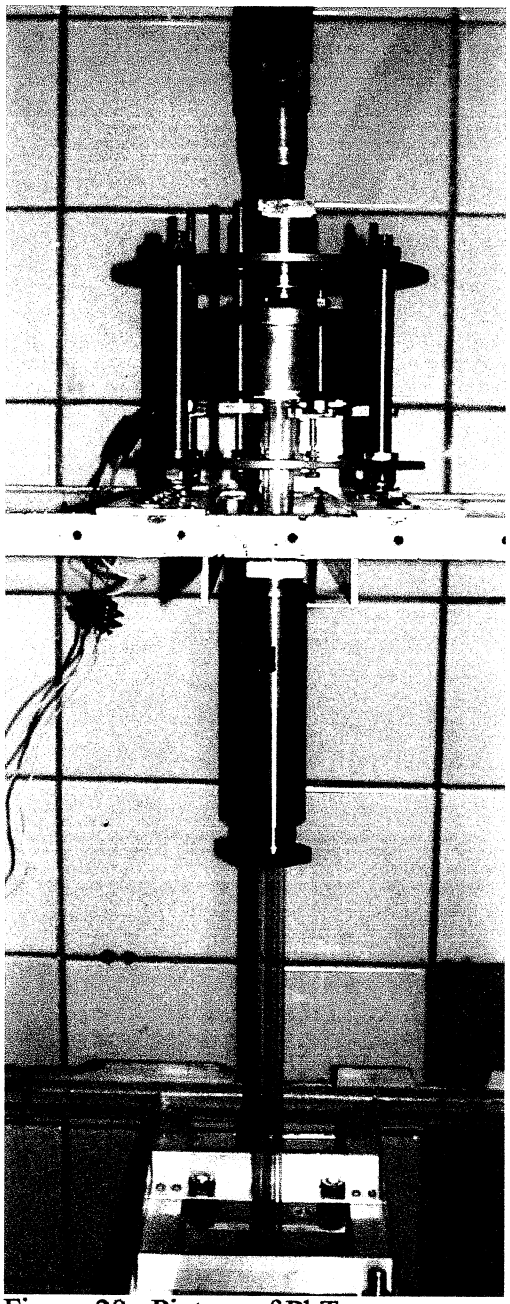

Figure 20. Picture of PbTe system

A schematic of the second generation system is shown in figure 19 and a picture of the system is in figure 20. Parts labeled 1-14 in figure 19 are as follows: 1)vacuum valve, 2) body of blade seal, 3) nut of blade seal, 4) electromagnetic mechanism, 5) rubber seal ring, 6) vibrating rod, 7) ampoule, 8) vibrating disk, 9) melt, 10) crystal, 11) heat transmitting rod, 12) steady magnet, 13) dielectric cylinder, 14) resistance furnace. The second generation furnace allowed for complete atmosphere control inside of the reactor, including the possibility for a vacuum. An electromagnetic device was used to implement vibrations over a frequency range of 10-200 Hz and an amplitude range of 0-0.5 mm. The system

allowed for the incorporation of various ampoule materials and had a maximum operating temperature of 1500°C.

The vibrating disk (8) is connected by the rod (6) to a fixed magnet (12), which was suspended in the field of external magnets (4). An alternating current with desired frequency was fed to the electromagnet in order to vibrate the disk. The electrical current determines the vibrational amplitude. To control the vibrating amplitude we used an auxiliary electromagnetic coil for feedback. The growth ampoule (7) was detachable and could be made from any close-grained crystalline ceramic, glass, quartz glass or metal (Pt, Ir, etc.).

3.4 Software for Fluid Flow Analysis

Special software was written in Moscow in order to process the video images of fluid flow in both CVS and AVC systems. The block scheme of the program is shown in figure21 and the user interface in figure 22.

A sequence of video frames (real-time AVI-format movie playing in area 10 in figure 22) is captured and digitized. Several frames are then layered in order to form a map of the flows. The combined image is filtered to remove steady objects like the heating spiral, splotches, non-moving particles, etc. This map is very similar to streak photography taken with a still camera, but has the advantage of being able to select the desired frames from the video tape. In this manner the video can be scanned for interesting segments, then these segments can be further analyzed. After mapping the flows, the flow velocities in different parts of the melt were calculated.

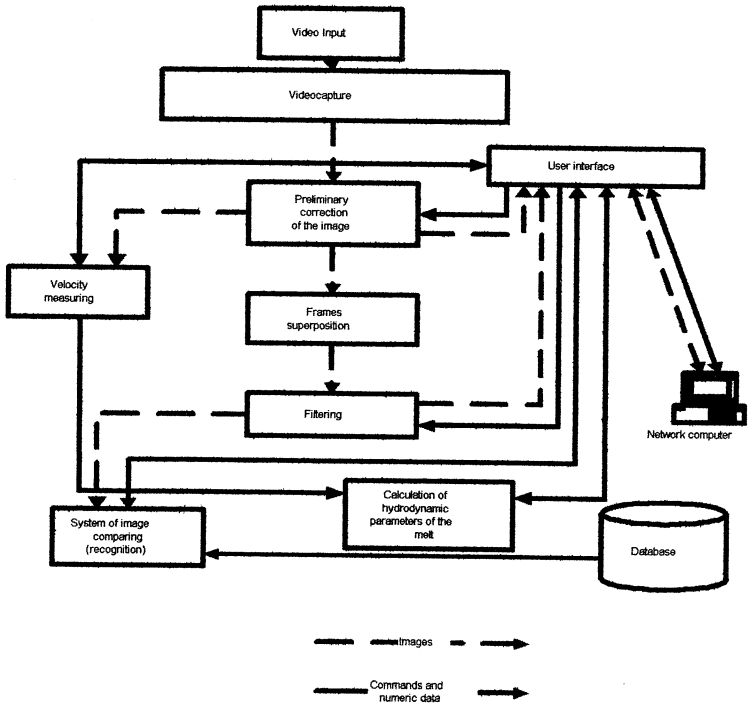

Figure 21. Block scheme for flow analysis program

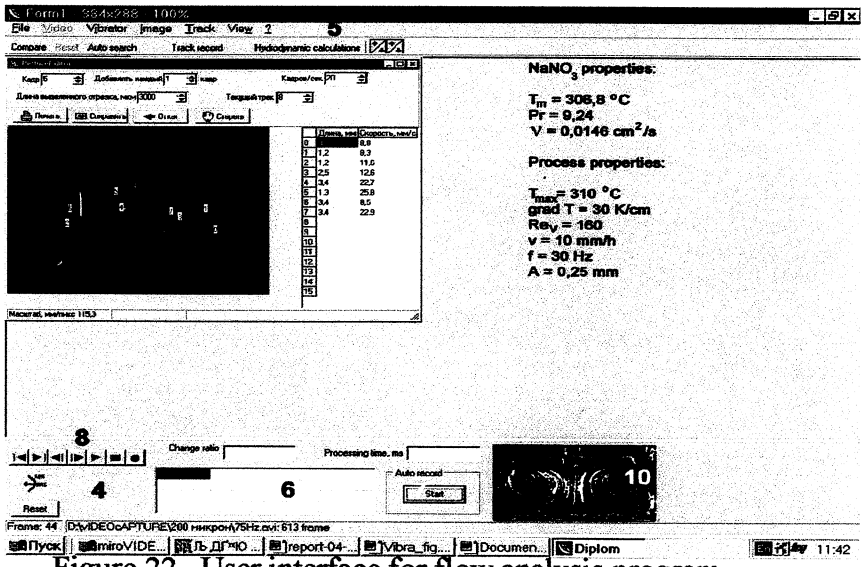

Figure 22. User interface for flow analysis program

The first step in determining flow velocity was to pick the appropriate scale for the system (most easily provided by a ruler in the image). In the traditional method of photo image analysis, the track length and exposure time are used to calculate the speed. Usually, there is no way of determining if the track is formed by a single particle. Contrary to the traditional technique, we marked the particle position manually on every frame. The particle speed was calculated using the values of frame speed, track length and the particle coordinates. Using the data obtained together with the physical properties of the melt, we calculated the hydrodynamic properties of the melt (area 1 on fig.22). Using this program, dynamic data for the flows was obtained.

4.0 Results and Discussion

4.1 Mathematical Modeling

4.1.1 AVC

Mathematical modelling of fluid flow behavior under AVC type vibrations was performed on the basis of the axisymmetric unsteady Navier-Stokes-Boussinesq equations for incompressible fluids. By using mathematical models, the influence of vibrational flow on boundary layers in Bridgman crystal growth and on heat and mass transfer during crystal growth was studied.

4.1.1.a Equations and Assumptions Used

The applied vibrations were assumed to be of small amplitude, therefore making the vibrator displacements negligible (typical AVC vibrational amplitudes are on the order of 0.1 mm). The velocity of the vibrator was defined as a harmonic function: $v = a\omega \sin(\omega t)$, where a is the amplitude, ω is the frequency, and t is time. A schematic of the system and variables used for the calculations is shown in figure 23.

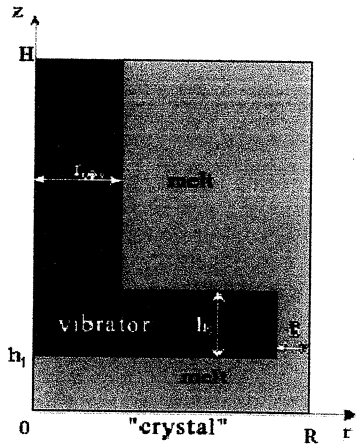

Figure 23. Schematic of system and variables used for calculations

The finite element code ASTRA [21-22] was used to make the calculations. In order to simplify the results, the calculated instantaneous flow velocities were averaged in time to create a parameter called average vibrational flow (AVF).

The two dimensional axisymmetric Navier-Stokes-Boussinesq equations for this system, including the heat and mass balance equations, are as follows:

$$\frac{\partial u}{\partial r} + \alpha \frac{u}{r} + \frac{\partial w}{\partial z} = 0 \tag{1}$$

$$\frac{du}{dt} - \alpha \frac{v^2}{r} = -\frac{1}{\rho}\frac{\partial p}{\partial r} + \frac{1}{r^{\alpha}}\frac{\partial}{\partial r}\left(r^{\alpha}\nu \frac{\partial u}{\partial r}\right) + \frac{\partial}{\partial z}\left(\nu \frac{\partial u}{\partial z}\right) - \alpha\nu \frac{u}{r^2} \tag{2}$$

$$\frac{dw}{dt} = -\frac{1}{\rho}\frac{\partial p}{\partial z} + \frac{1}{r^{\alpha}}\frac{\partial}{\partial r}\left(r^{\alpha}\nu\frac{\partial w}{\partial r}\right) + \frac{\partial}{\partial z}\left(\nu\frac{\partial w}{\partial z}\right) + g\beta(T - T_0) \tag{3}$$

$$\frac{dv}{dt} + \alpha\frac{uv}{r} = \alpha\left[\frac{1}{r}\frac{\partial}{\partial r}\left(r\nu\frac{\partial u}{\partial r}\right) + \frac{\partial}{\partial z}\left(\nu\frac{\partial u}{\partial z}\right) - \nu\frac{u}{r^2}\right] \tag{4}$$

$$\frac{d\rho c_p T}{dt} = \frac{1}{r^{\alpha}}\frac{\partial}{\partial r}\left(r^{\alpha}\lambda\frac{\partial T}{\partial r}\right) + \frac{\partial}{\partial z}\left(\lambda\frac{\partial T}{\partial z}\right) \tag{5}$$

$$\frac{dC}{dt} = \frac{1}{r^{\alpha}}\frac{\partial}{\partial r}\left(r^{\alpha}D\frac{\partial C}{\partial r}\right) + \frac{\partial}{\partial z}\left(D\frac{\partial C}{\partial z}\right) \tag{6}$$

with the boundary conditions of:

axis of symmetry (r=0): $u=0,\ \frac{\partial w}{\partial r} = 0,\ v=0,\ \frac{\partial T}{\partial r} = 0,$ (7)

solid-liquid interface (z=0): $u=0,\ w = -W_s,\ v = 2\pi r\Omega_c,\ T=T_m,\ D\frac{\partial C}{\partial z} = W_s C(1 - k_0)$ (8)

side wall of crucible (r=R): $u=0,\ w=0,\ v=2\pi r\Omega_c,$ (9)

$\frac{\partial T}{\partial r} = 0$ ($0<z<h$), $T=T_H$, ($h<z<H$), $\frac{\partial C}{\partial r} = 0$; (10)

vibrator: $u=0,\ w = A\ \omega\ \sin(\omega\ t),\ v = 2\pi r\Omega_{vibr},\ \frac{\partial C}{\partial n} = 0,\ \frac{\partial T}{\partial n} = 0$ (11)

upper opened boundary (z=H): $u=0,\ \frac{\partial w}{\partial z} = 0,\ v=0, T=T_H,\ C=C_o$ (12)

Initial conditions (t=0) : $u=0,\ w=0,\ v=0,\ T=T_m,\ C=C_o$ (13)

where r and z are radial and axial coordinates, t is time, u and w are velocity vector components in the r and z directions, v is azimutal velocity, T is temperature, C is dopant concentration, p is pressure, ρ is density, g is gravity acceleration, β_T is the coefficient of thermal expansion, ν is kinematic viscosity, λ is thermal conductivity, C_p is heat capacity, D is dopant diffusivity, α is the geometry factor, which is equal to 0 for flat geometry and to 1 for axisymmetrical problems, A is amplitude of vibration, ω is frequency of vibration, Ω is angular velocity of a rotating crucible, a is the thermal conductivity coefficient, W_s is rate of the crystal growth, ΔT is change in temperature, k_o is the dopant segregation factor, n is the normal unity vector, R is the radius of the crucible.

The crystal growth rate was the same in all simulations: $W_s = 0.3$ cm/h and the amplitude of vibrations was constant A=100μm. This problem is characterized by the following dimensionless parameters: the rotational Reynolds number $Re_\Omega=\Omega_C R^2/\nu$, the Reynolds number $Re=W_S R/\nu$, the vibrational Reynold's number $Re_{vibr}=A\omega R/\nu$, the Grashof number $Gr=g\beta\Delta T R^3/\nu^2$, the Rayleigh number Ra = GrPr, the Prandtl number $Pr=\nu\rho C_p/\lambda$ and the Schmidt number $Sc=\nu/D$.

4.1.1.b Numerical Results

Equations 1-13 were solved using ASTRA to predict AVC flow behavior and its effect on the thermal boundary layers. The effect of changing vibrational frequency on the fluid flow is shown in figure 24. Figure 24 shows constant velocity (AVF) lines for four different vibrational frequencies. As vibrational frequency is increased, the velocity of the flows produced likewise increase. Secondary flow cells can also form as can be seen below the piston in figure 24 b) and 24 c). It can be seen that by increasing the frequency from 10 Hz to 100 Hz, the flow direction was changed from counterclockwise to a clockwise direction as a secondary flow cell grew and eventually overcame the primary cell.

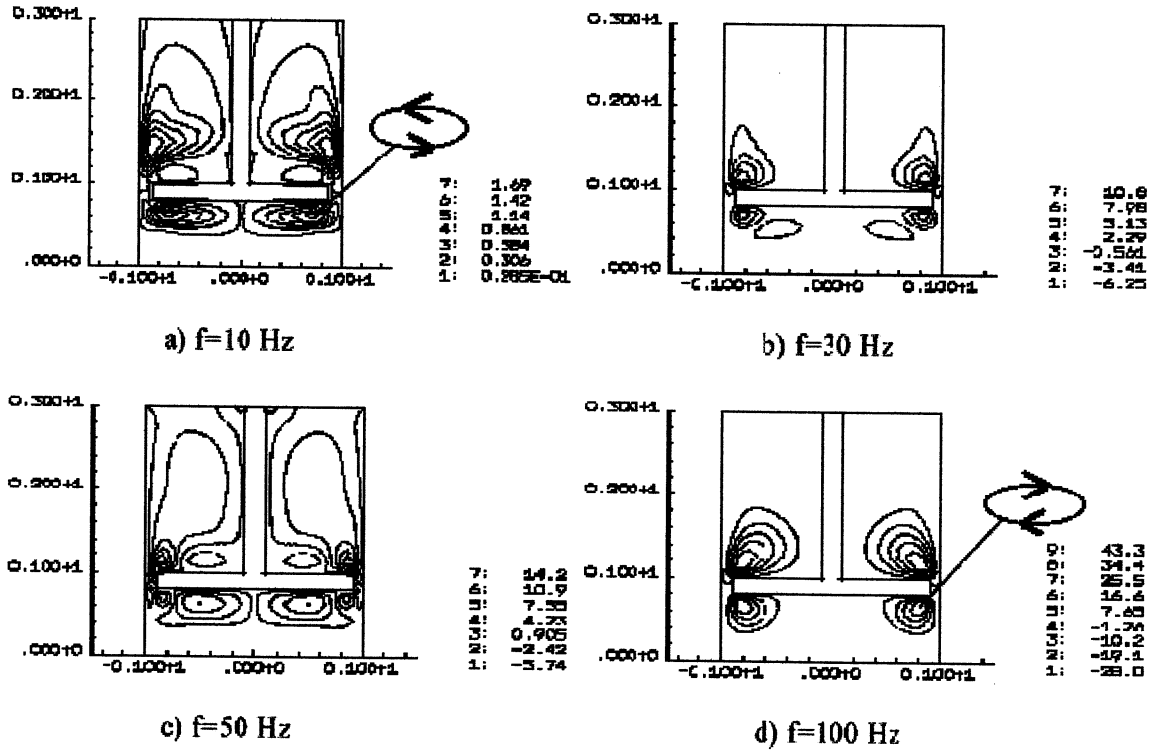

a) f=10 Hz

b) f=30 Hz

c) f=50 Hz

d) f=100 Hz

Figure 24. Influence of vibrational frequency on fluid flow

Some simulations were performed in which the baffle was rotated as well as vibrated. The results from these experiments showed that the rotation helped to level the radial temperature distribution.

Figure 25 shows the influence of vibrational flows on the thermal boundary layer in a system with Gr=2.1 x 10^6, Pr=5.43, and H/R=3.2. The thermal profile on the bottom left (no vibrations) shows a much wider thermal boundary layer than the lower right thermal profile (vibrations at 50 Hz frequency and 100 μm amplitude). The stream functions of flow can be seen above the thermal profiles. The convective flow present without vibrations is not strong compared to vibrational flow under these conditions. The AVC generated flows are much stronger than the buoyancy driven convective flows and as a result, reduce the thermal boundary layer thickness.

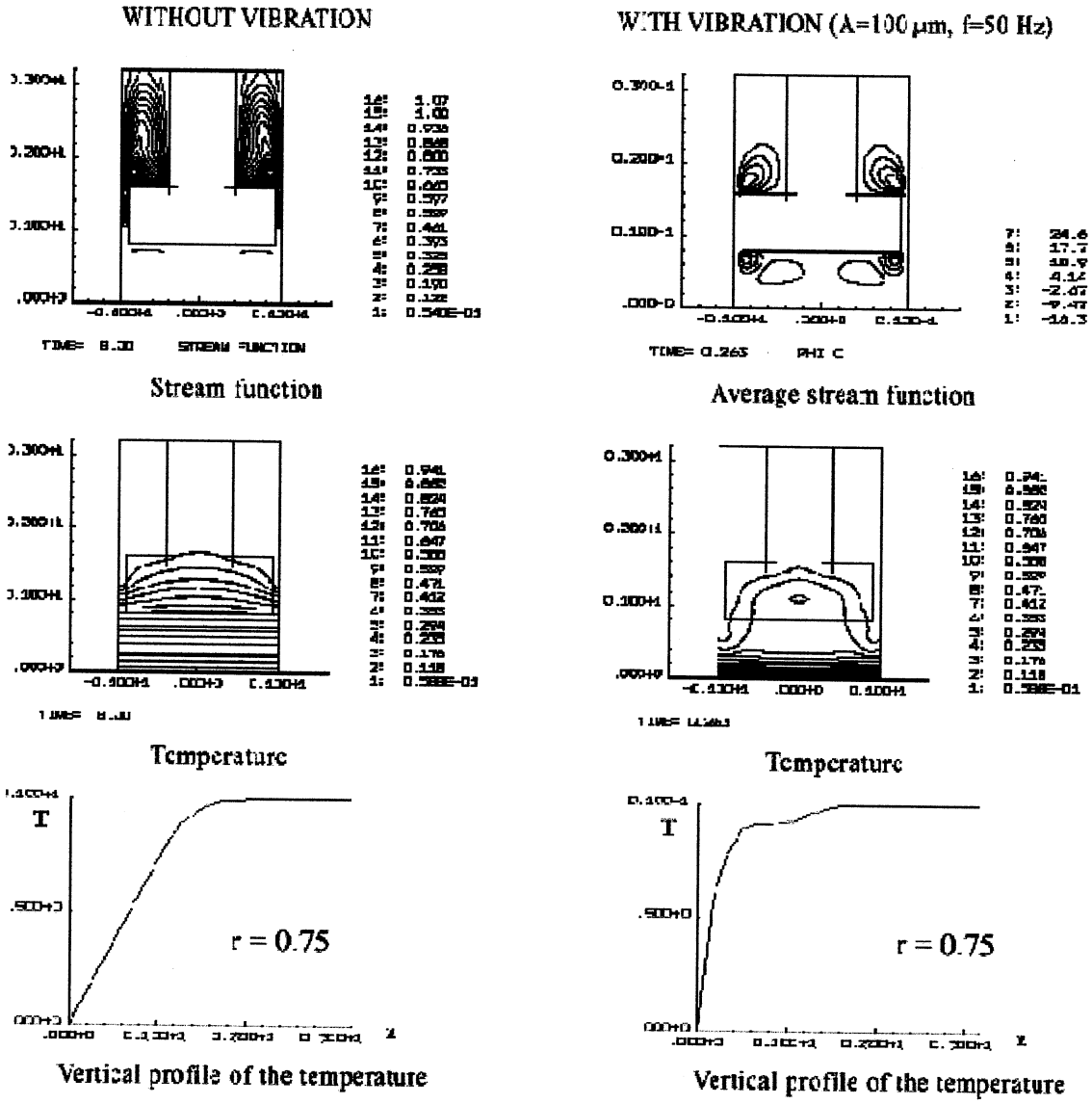

Figure 25. Effect of AVC flows on thermal boundary layer thickness

In summary, the mathematical modeling shows that by changing the frequency of vibration, flow intensity and direction can be manipulated as well as the thermal profile of the system. Simulations found this to be true in both terrestrial and microgravity environments.

4.1.2 CVS

As stated in the experimental procedure section, the CVS method, like AVC, involves a number of important parameters. The independent variables include vibrational, geometric, and fluid parameters (figure 26). The vibrational parameters for the setup described previously in the experimental procedure are the frequency (ω) and amplitude (a). The important geometric parameters for crucibles of cylindrical geometry are the crucible diameter (d) and the aspect ratios (AR), in this case, liquid height to crucible diameter. The viscosity (μ), density (ρ), and kinematic viscosity (ν) are important fluid parameters. The CVS method produces non-axisymmetric flows by using a free surface. This type of flow is very difficult to model mathematically.

Even though directly relevant computational mathematical predictions could not be made, a simple mathematical model was derived in order to determine the size of upward and downward flow regimes observed in the CVS physical modelling system. A mass balance was used along with the assumptions of a constant density liquid and seperate regions for upward and downward flow in a cylindrical geometry (figure 27) in order to derive the following expression which relates the internal radius (r_i) to the ampoule radius (r_o) and the ratio of the magnitude of the upward velocity to the downward velocity (v_{up}/v_{down}): $r_i = r_o\left(\frac{v_{up}}{v_{down}} + 1\right)^{\frac{-1}{2}}$

This expression can be used to determine approximate shapes of the upward and downward flow regions based on velocity measurements and the ampoule radius. In the case of the particle tracer experiments (discussed later) where velocity was measured, an

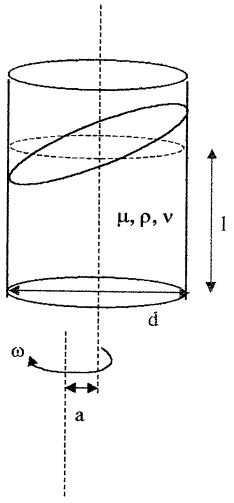

Vibrational Parameters
- amplitude (a)
- frequency (ω)

Geometric Parameters
- crucible diameter (d)
- liquid height (l)
- aspect ratio (AR = l/d)

Fluid Parameters
- viscosity (μ)
- density (ρ)
- kinematic viscosity ($\nu=\mu/\rho$)

Figure 26. Schematic of system with important variables

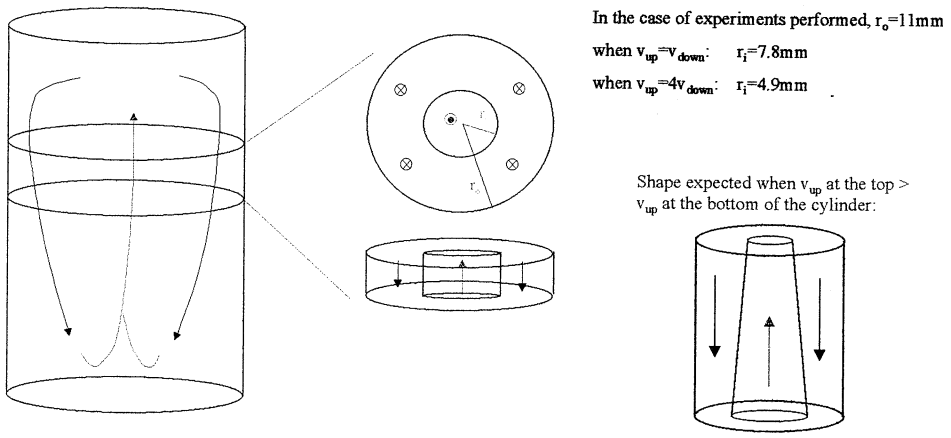

Figure 27. Setup for mass balance and results of applying derived equation

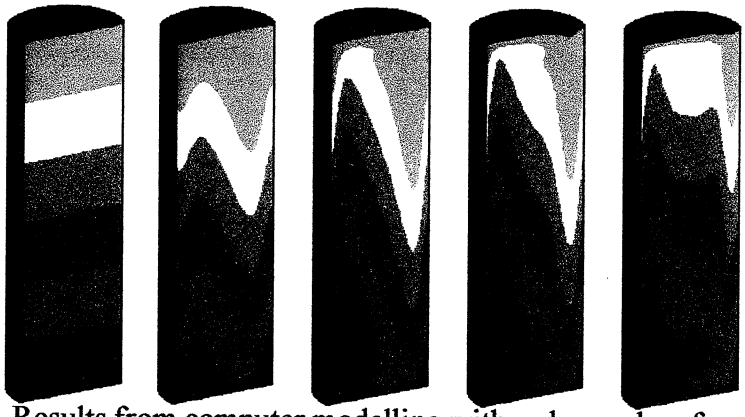

Figure 28. Results from computer modelling with a clamped surface depicting a thermal gradient being mixed using vibration induced flows [23]

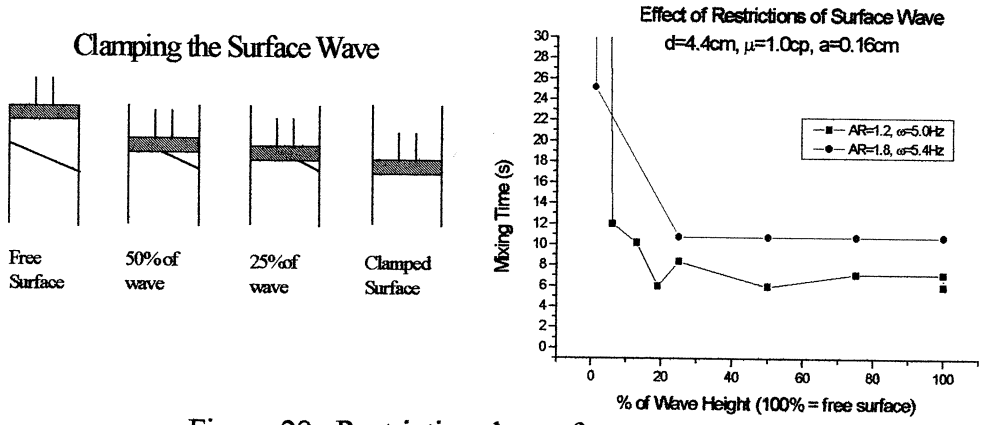

Figure 29. Restricting the surface wave

ampoule radius of 11 mm was used. Under this condition, the upward velocity region has a radius of 7.8 mm when the upward and downward velocities are equal. The upward velocity region shrinks to a radius of 4.9 mm when the downward velocity is 1/4 of the upward velocity. The trucated cone shaped boundary as shown in figure 27 results from the ratio of upward to downward velocity decreasing with depth from the surface. This model is a first order approximation that does not take into consideration a finite boundary layer thickness or interactions between upward and downward flows. The model provides some insight as to what is happening in the CVS system, even though during observations of the physical modelling system, interactions between upward and downward flows at the flow boundaries could be observed at various depth levels.

One of the original program goals was to verify and refine the theoretical predictions derived from the mathematical modelling work of A. Fedoseyev and I. Alexander. They were working under NASA grant No. 95-346. Although Fedoseyev and Alexander's work [14] dealt with a similar method to introduce vibrations to a melt, they did not work with a free surface (no surface wave) in order to be able to perform the finite element calculations. Fedoseyev indicated [24] that a large temperature or density gradient in our system should produce significant mixing even without a surface wave. An example of their results on the influence of vibrations on a temperature gradient is shown in figure 28.

In order to compare our physical modelling results directly to their predictions, we devised a method to clamp the surface wave with a plastic piston inserted to the top of the ampoule. Unfortunately, the gradients required by Fedoseyev's mathematical predictions (temperature gradients on the order of 50-100°C/cm) were too large to be produced experimentally. When the surface wave was completely clamped, no fluid motion was observed under any CVS conditions. However, if even a small bubble of air was trapped under the clamp, mixing would occur although at a slower rate than with a free surface. Several dye experiments were performed to study the effect of restricting the height of the surface wave. Figure 29 shows that CVS mixing time is fairly constant until only a small amount of air is present above the liquid (~1% of the wave height is left). This suggests that a type of inertial force produced by the motion of the free surface, rather than the wave height itself, is the primary mixing force.

4.2 Low Temperature Modeling (No melt or temperature gradient)

4.2.1 AVC

The water/glycerin system was used to determine how AVC flows differed in a microgravity and terrrestrial environment. The flow analysis software developed in Moscow was used to compare the average vibrational flow velocity for terrestrial and microgravity environments. As previously seen, AVC generated flow velocities are position dependent with respect to the ampoule boundaries and the vibrator position. In order to make a relevant comparison of flow velocities generated under different conditions, a standard position to measure velocity was chosen at 5 mm below the vibrating disk on the central axis . This position allowed for maximum accuracy in flow velocity measurement due to a minimization of optical distortion effects.

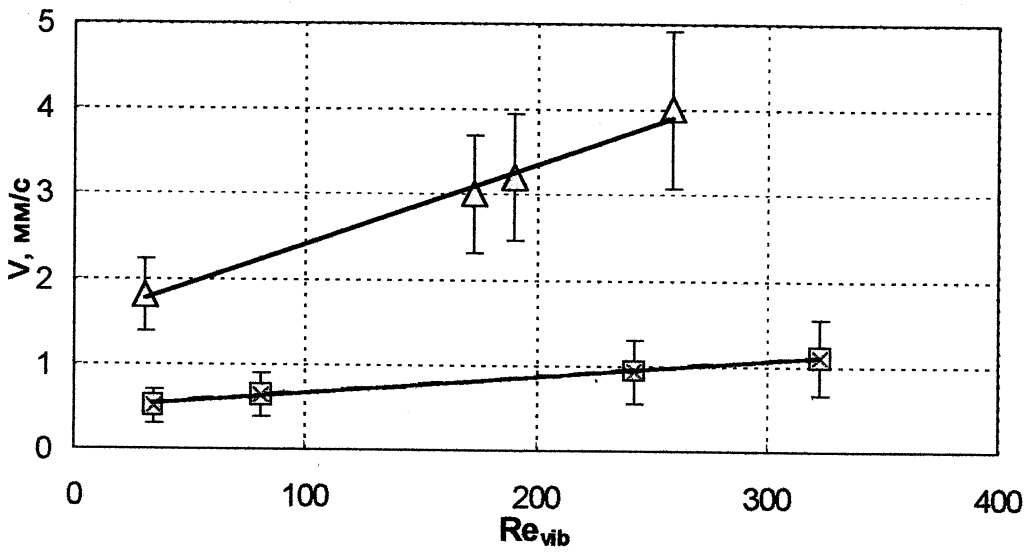

Figure 30. AVF velocity versus vibrational Reynold's number

Figure 30 shows a plot of velocity in mm/s versus the vibrational Reynold's number for both the terrrestrial (square points) and the microgravity (triangle points) experiments. The fluid used in this experiment was a water/glycerin solution (60vol% glycerin), and the experiment was performed at room temperature. In both terrestrial and microgravity cases, velocity increases with increasing vibrational Reynold's number. However, the velocity in the microgravity environment is higher than terrestrail conditions for a given vibrational Reynold's number and increases at almost twice the rate of the terrrestrial experiments.

Based on this data, the AVC flows are enhanced in a microgravity environment. Less energy is required to produce flows in a microgravity environment of the same magnitude as seen on earth. This suggests that graviational forces work against the fluid flow created by AVC.

4.2.2 CVS

The water/glycerin system was used to examine how the mainpulation of the variables listed in the mathematical modelling section affect fluid flow in the CVS system. The dependent variables measured in this study included: fluid mixing time (t), wave height (h), resonance frequency (Ω), depth of flow from fluid surface (ϕ), and the fluid velocity (v).

4.2.2.a Mixing Time and Wave Height

The first study on CVS by Liu et al. [13] contained preliminary data showing how t and h were dependent on ω, d, AR, and μ. Because the original study was performed approximately 10 yrs before the start of this program and experiments on the system were not ongoing in this timeframe, the first step taken was to verify the original results. The newly generated data was found to match the literature data, and the data set was expanded to include a wider range of previously studied parameters. In the current study, the effect of

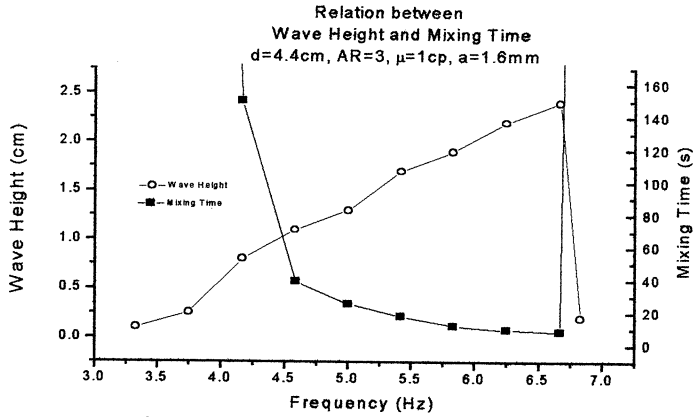

Figure 31. Typical mixing time and wave height as a functior vibrational frequency

varying the vibrational amplitude was also examined. The amplitude was not found to have a large effect on t or h, however smaller amplitudes were found to have smaller resonance frequencies (defined below).

Data showed that as the wave height increased, mixing time decreased (figure 31). In most experiments, the wave collapsed at a specific frequency (the resonance frequency) causing a dramatic change in flow behavior and a corresponding increase in mixing time. The resonance frequency thus defines the frequency at which maximum flow can be acheived in a given system. The wave did not collapse however for ampoule diameters of 3.2 cm or smaller and viscosities near 1.0 cp, regardless of frequency, giving no limitation on the maximum flow condition for these systems.

Because mixing still occurs even when the surface wave is clamped (section 4.1.2), the surface wave does not seem to be the primary driving force, but rather a measure of the energy input to the system and the energy state of the system. The wave height increases as more energy is added to the system, and mixing times decrease as a result of the extra energy. The resonance frequencies can be used to define the energy state of the system

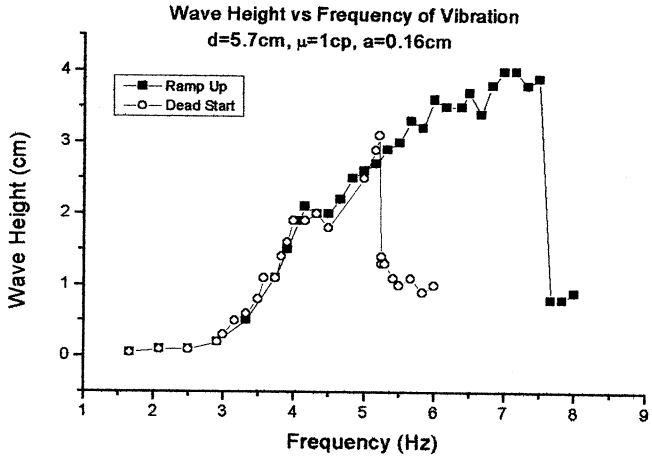

Figure 32. Typical wave height versus frequency shov ing dependence on system history

with collapsed waves and their corresponding slower mixing times being at a different energy state than the precessing surface wave.

The CVS system was found to exhibit hysteresis-like behavior with regard to the wave height and resonance frequency measurements. If the frequency was slowly increased from the rest state, then a wave could be present, though unstable, well beyond the resonant frequency (figure 32). If the vibrations were initiated immediately at the desired frequency (dead start), then the wave always collapsed at the same frequency. This effect is believed to be due to system inertia. Once the flows in the system were started and increased (incrementally), the inertia of the swirling flows in the fluid support the unstable wave.

4.2.2.b Effect of Frequency and Viscosity on Velocity and Depth

To expand our understanding of CVS generated flows, including the effect of frequency and viscosity on fluid velocity and the depth reached by the flows below the surface wave, neutrally buoyant particles were added to the water/glycerin solutions. Figure 33 shows a series of streak photographs of the flows generated between 5.0 and 6.7 Hz in a system with the parameters d=2.2 cm, a=0.16 cm, and μ=1.0 cp. A 1/60 s film exposure time was used. Longer streaks corresponded to faster moving particles. At 5.0 Hz, only the top ~2cm of fluid show any motion. At 5.4 Hz, flows have reached deeper into the fluid, and by 5.8 Hz particle motion has reached to the bottom. Estimates of particle velocity can be made from such pictures by using the streak length and exposure time. The velocity calculations are estimates because the particles are moving in three dimensions and the camera only sees motion in a plane. At a depth of 3.6 cm from the fluid surface, particle velocities for the five photographs from left to right were estimated at 0 mm/s, 15 mm/s, 46 mm/s, 92 mm/s, and 92 mm/s. Data such as this shows that a small change in vibrational frequency has the potential to cause a large change in average fluid velocity at a given depth from the fluid surface.

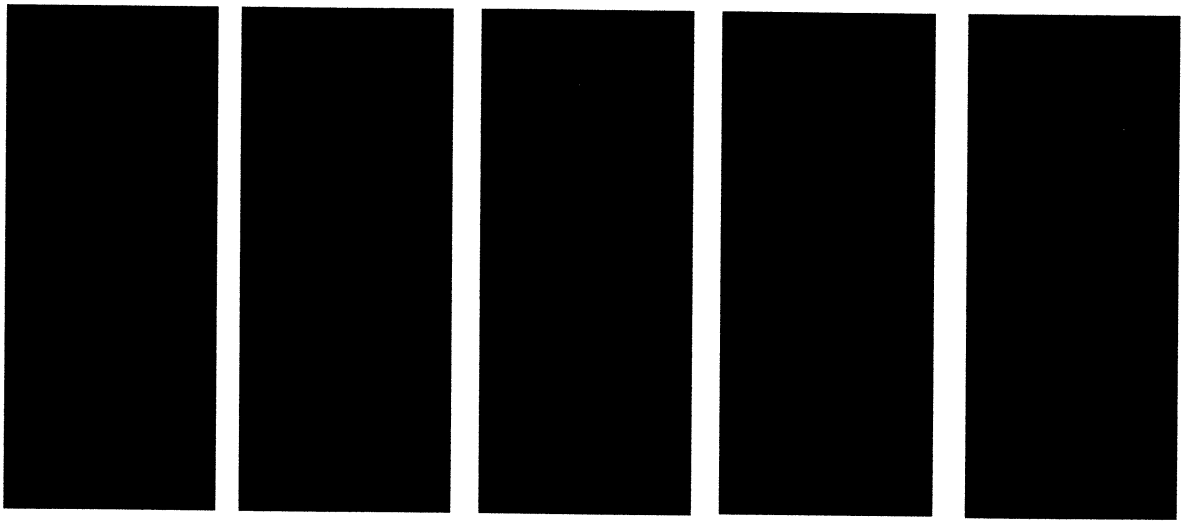

Figure 33. Streak photography of CVS flows (d=2.2cm, μ=1.0cp, a=0.16cm, 1/60s exp.)

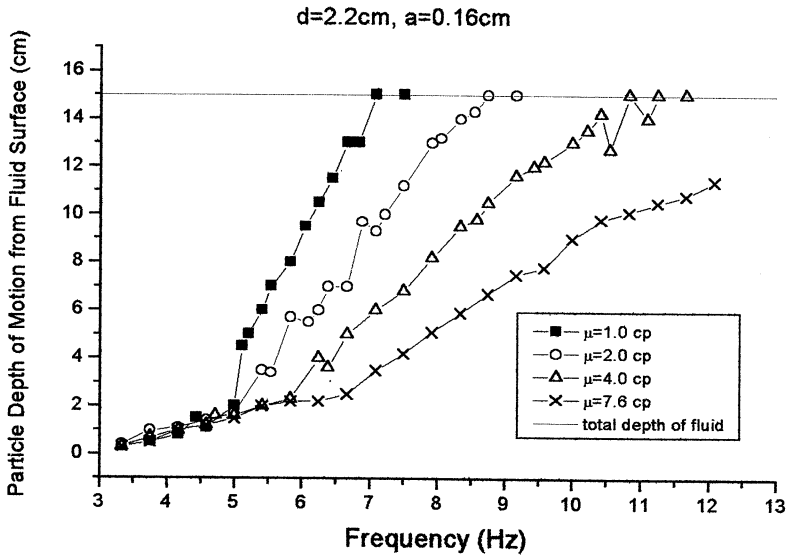

Figure 34. Depth of fluid motion versus frequency and viscosity

The depth dependence of fluid flow can be very important in Bridgman type systems. During typical Bridgman growth the depth of the melt is constantly decreasing as the crystal is grown. A depth of motion plot could be a valuable tool in determining how to maintain a constant flow level in the system. Figure 34 shows a plot of motion depth versus vibrational frequency for several different viscosities. The depth of motion in this plot is defined as the depth at which particles are stationary with respect to the moving ampoule, or where the flows driven from the surface stop moving. For example, at a frequency of 6 Hz the depth will be only 2 cm below the surface if the viscosity is 7.6 cp, but about 10 cm for a fluid viscosity of 1 cp. For the higher viscosity solution to reach the latter depth, a frequency of 10 Hz would be required. Because the depth of motion is very sensitive to viscosity, knowledge of the viscosity of the melt or a reasonable estimate is important to the application of this data to a real growth system.

The CVS generated flows take time to be driven from the surface into the fluid. The flows can take up to a few minutes to reach their steady state conditions. Figure 35 shows the time dependence of motion depth for several frequencies of vibration. Steady state flow did not occur at the same time at all frequencies. As the frequency increased, the time to reach steady state flow decreased from approximately 55 s to 30 s. In one minute the flow depth for the higher frequency was ~50 mm while that of the lowest frequency was only ~10 mm.

Velocity profiles for the fluid were obtained using software developed in Moscow. The velocity profiles obtained showed that on average the particles near the top of the fluid are moving faster than particles at the bottom (figure 36). Wide variations in velocity seen near the fluid surface may be accounted for by the erratic nature of the flows near the surface wave, and also by the fact that the camera is only seeing two of the three dimensions.

The velocity profiles in figure 36 match well with the depth of fluid motion plotted in figure 34. Figure 34 shows that a 1.0 cp fluid at 5.42 Hz and a 3.0 cp fluid at 6.25 Hz both reach the same depth of 5.0 cm, and figure 36 shows the fluid velocity in both cases

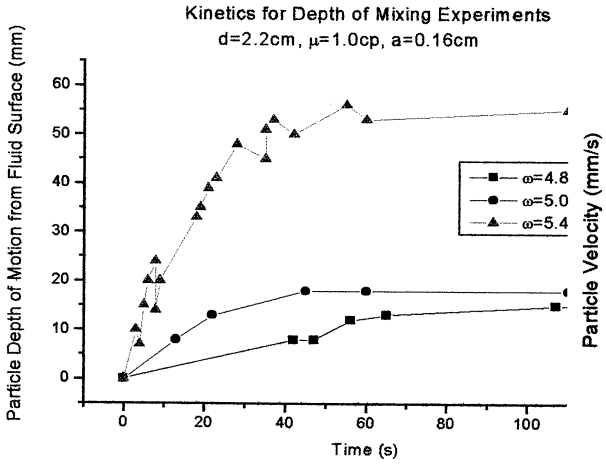

Figure 35. Time dependence of depth of m ing for several frequencies

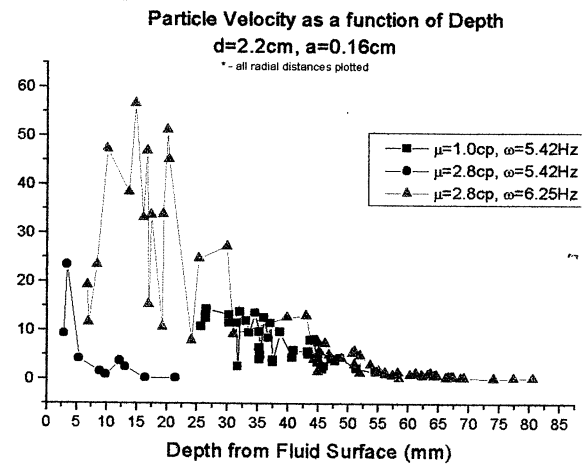

Figure 36. Particle velocity as a function of depth in fluid

approaching zero near 5 cm. A 3.0 cp fluid at 5.42 Hz reaches a depth of 2.0 cm according to figure 34, which corresponds well with figure 36 where the fluid velocity for this case also approaches zero near 2 cm.

If the large variations in velocity seen near the surface wave are real (not an artifact of seeing only 2 of 3 dimensions), then such fluctuations could cause problems during crystal growth if the interface is close to this region. In order to maintain stable growth, it would be better if a more stable flow region, such as found further into the fluid (near where flows stop) could be positioned near the growth interface. In Bridgman growth, the interface moves toward the fluid surface during growth. Therefore, in order to keep a given flow region near the interface, the frequency would have to be lowered as growth proceeds.

4.2.2.c Damping Flows

A key point obtained from the CVS velocity profiles was that flow rates are not constant throughout the fluid. One proposed application of CVS was to use this technique in order to damp undesirable flows such as those produced through natural convection or 'g-jitter.' CVS could be used to damp flows but only over a limited length of the fluid as defined by the region where the flows are of equal magnitude but opposite direction. In principle, CVS could be set to a frequency which would damp flows near the solid/liquid interface (the region where undesirable flows can be most harmful to crystal growth), then this frequency could be ramped back according to the depth of motion curves as the crystal grew.

An experiment was performed to check the ability of CVS to damp flows. A propeller mixing blade (2.25 cm blade length) was inserted into an ampoule (4.4 cm diameter) containing water (15.5 cm depth) and tracer particles. The mixer was run with a DC power source and was positioned 8.2 cm from the fluid surface. The mixer was set to produce clockwise flows which were the opposite direction of the counter-clockwise CVS generated flows. By correctly setting the CVS frequency, a small damped region

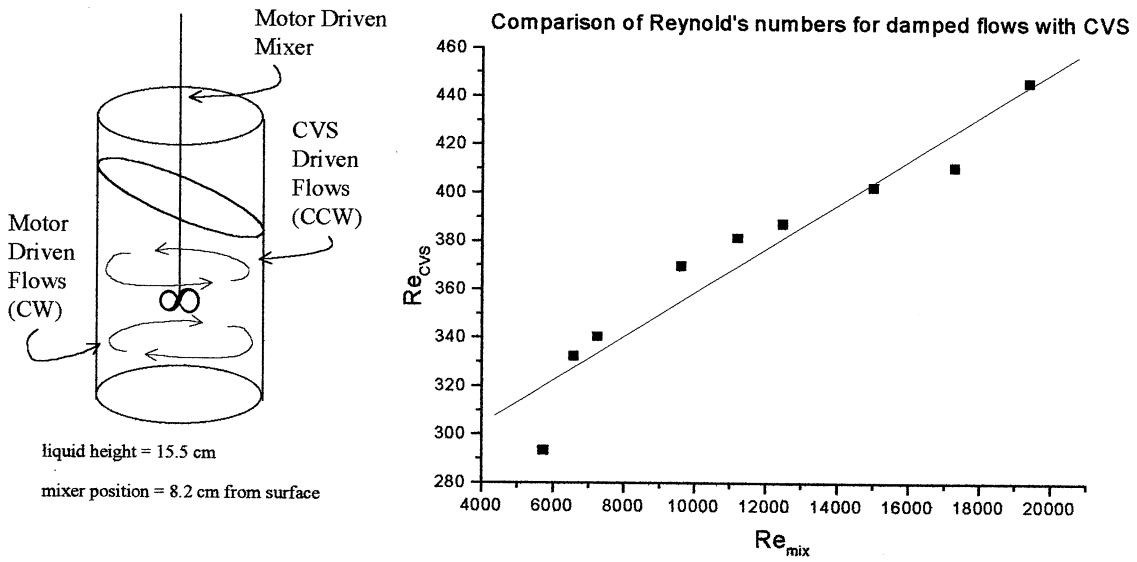

Figure 37. Setup and results from flow damping experiment

(between 0.5 and 1.0 cm long) could be produced with mixer induced flows below and CVS induced flows above. By adjusting the frequency of vibration, the damped region could be moved through the ampoule. Figure 37 shows a comparison of the Reynold's numbers required to reverse flows at the region just above the mixer blade. The CVS and mixer Reynold's numbers are defined as follows: $Re_{CVS} = (\omega a d \rho)/\mu$ and $Re_{mix} = (f D_a^2 \rho)/\mu$ where ρ is the fluid density, f is the rotational frequency of the mixer, and D_a is the mixer blade length.

4.3 Low Temperature Modeling using $NaNO_3$ Melts

4.3.1 AVC

Sodium nitrate was used to determine the effects of AVC generated flows on growth interface shape, crystal quality in the form of dislocation densities and x-ray topographs, and dopant segregation.

When AVC vibrations were initiated in the $NaNO_3$ melt, the solid liquid interface typically would melt back (similar to the meltback effect seen in CVS) from 1 to 5 mm. The position of the vibrating disk was adjusted accordingly in order to maintain a constant distance from the growth interface.

4.3.1.a Growth Interface Shape

By adjusting vibrational parameters, the growth interface shape could be altered. Figure 38 shows how interface curvature was manipulated by changing the vibrational Reynold's number for three different frequencies. A positive curvature indicates a convex interface, and a negative curvature indicates a concave interface. Vibrational Reynold's

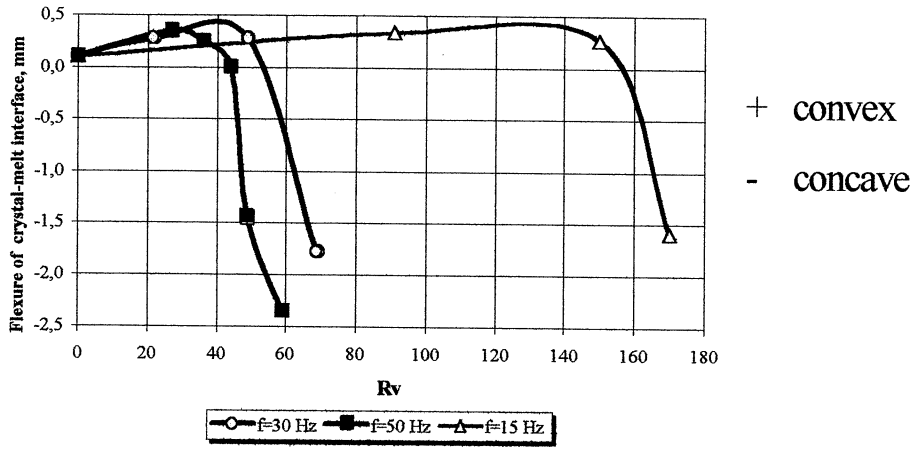

Figure 38. Interface curvature versus vibrational Reynold's number for 3 frequencies

number was altered by changing the vibrational amplitude over a range of 0.08-1.2 mm for each frequency.

At small vibrational amplitudes (low vibrational Reynold's numbers), an amplitude increase results in a slight increase in interface convexity. Beyond a critical amplitude, the interface shape rapidly becomes concave. By appropriately adjusting the vibrational parameters, a wide range of interface curavtures could be produced, including a flat interface for each of the frequencies studied. A slight convexity to the interface is believed to provide improved crystal quality by causing defects to grow out of the crystal.

4.3.1.b Crystalline Quality

The crystal quality of AVC-grown crystals was examined by using dislocation density and x-ray topographs.

Dislocation densities were measured through a chemical etching technique. Alcohol was used to polish $NaNO_3$ crystals and a zinc acetate in acetic acid solution was used as an etchant. Figure 39 shows a plot of dislocation density (cm^{-2}) versus vibrational amplitude (μm). Both growth and induced dislocations decrease when vibrational amplitude increases. Induced disloactions include dislocations caused by grinding and polishing samples, as opposed to dislocations formed only during growth. The low dislocation densities obsevered at high vibrational amplitude are not common in $NaNO_3$ crystals. A similar decrease in dislocations with increased vibration was observed in the earlier studies mentioned previously in the background section. The mechanism is not known.

X-ray topography was also used as a technique to examine crystalline quality of AVC and non-AVC crystals. Figure 40 shows x-ray topographs of a) an AVC grown crystal and b) a non-AVC grown crystal. The AVC grown crystal exhibits more lattice distortion (dark regions) than the non-AVC grown crystal. The lattice distortions in both crystals seem to be mostly directed along the growth axis. The increased thermal gradients present at the

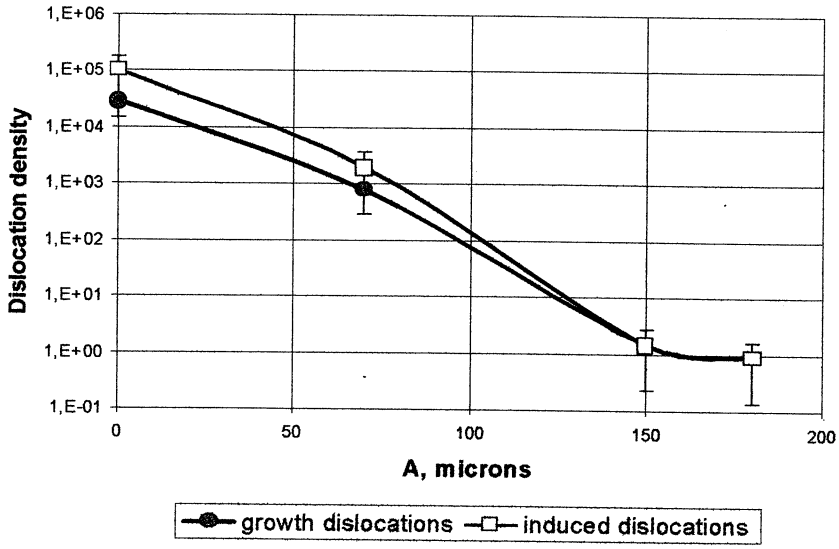

Figure 39. Dislocation density versus vibrational amplitude

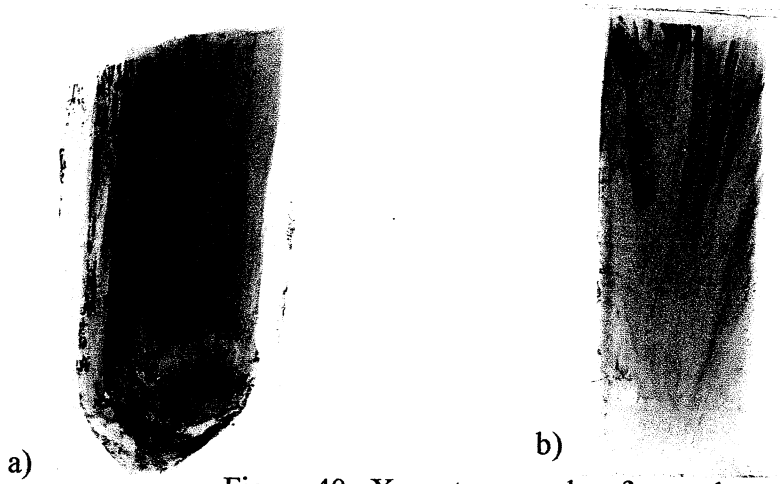

a) b)

Figure 40. X-ray topographs of crystals grown
a) using AVC and b) without AVC

growth interface in the AVC grown crystal provide a possible explanation for the increased lattice strain present. A similar result was observed by Lu et al. [15] in CVS grown CdTe.

4.3.1.c Ag doping of $NaNO_3$

In order to determine how AVC effects dopant distribution, sodium nitrate was doped with 1 wt% silver nitrate. Three crystals were grown using dopants. The first was grown using an ampoule translation rate of 2 mm/h and no vibrations. The other two were grown using an ampoule translation rate of 5 mm/h and a vibrational frequency of 50 Hz. One of these two was grown using a vibrational amplitude of 0.15 mm to create a more convex interface, and the other was grown using a vibrational amplitude of 0.20 mm to create a flat growth interface. The control sample was grown at 2 mm/h because a reasonable quality $NaNO_3$ crystal could not be grown at a faster rate under these experimental conditions without the aid of vibrations.

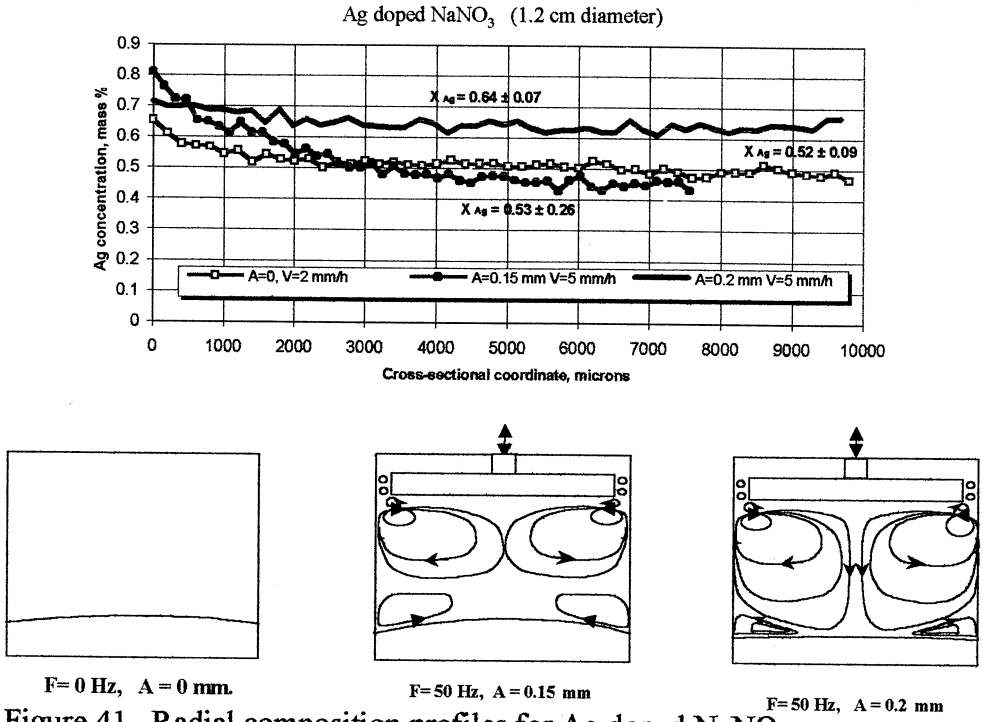

Figure 41. Radial composition profiles for Ag doped $NaNO_3$

Figure 41 shows radial concentration profiles for the three crystals. Schematics of the observed flows and corresponding interface shapes for each of the growth conditions are at the bottom of figure 41. The Ag concentration was measured using electron microprobe analysis (EPMA) in Camebax, France. Due to the soft nature of $NaNO_3$, the electron beam was widened to 15 μm to minimize sample damage. Pure silver nitrate was used as a standard.

The radial profiles obtained correlated well with visual observations of the interface shape during growth. The flatest radial profile was for the crystal grown with the flat interface (a = 0.2 mm) and contained an average silver concentration of 0.64±0.07. The crystal grown

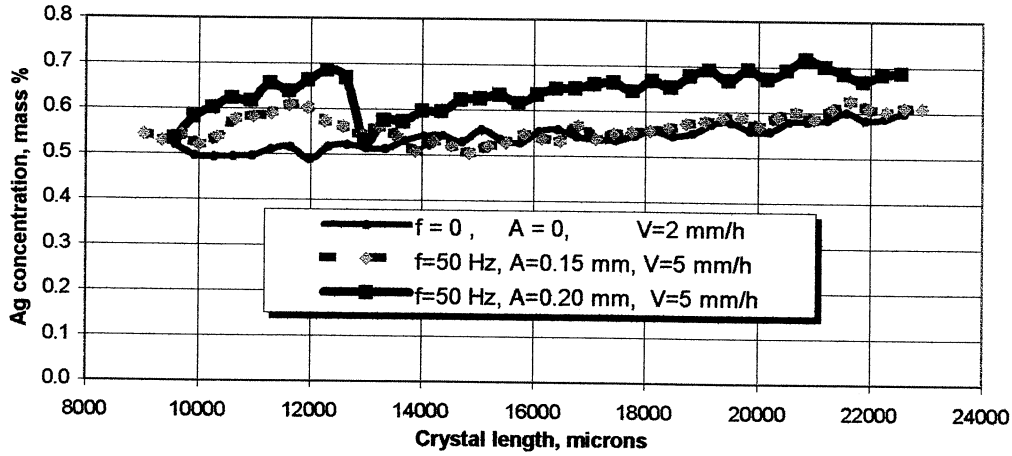

Figure 42. Axial concentration profiles for Ag doped $NaNO_3$

under a vibrational amplitude of 0.15 mm had the most convex interface and showed the most variation in concentration with an average silver concentration of 0.53±0.26.

Axial concentration profiles for the three crystals are given in figure 42. All crystals had axial concentration profiles typical of a material with a segregation coefficient less than one (K_{eq}^{Ag} =0.76) in that the Ag concentration increased along the growth direction. The concentration drop seen in the two crystals grown with AVC corresponds to the start of vibrations. When AVC induced flows began, the Ag distribution in the melt was changed and the diffusion boundary layer near the growth interface became smaller causing a change in Ag concentration in the grown crystal.

Effective segregation coefficients were calculated using the axial concentration profiles. The crystal grown without AVC had a calculated $K_{eff}^{Ag} = 0.88$ and the crystal grown with a frequency of 50 Hz and 0.20 mm amplitude had a calculated $K_{eff}^{Ag} = 0.78$. By applying vibrations, a segregation coefficient closer to that of the equilibrium value was acheived.

The Burton-Prim-Slichter equation describes the effective distribution coefficient (K_{eff}) in terms of the equilibrium segregation coefficient (K_o), the growth rate (f), the diffusion boundary layer thickness (δ), and the diffusivity in the liquid (D):

$$K_{eff} = \left(1 + (K_o^{-1} - 1)e^{-f\frac{\delta}{D}}\right)^{-1}$$

This equation shows that when f is increased holding everything else constant, K_{eff} should become closer to 1. In the AVC growth experiments, f should have been higher for the AVC growth versus the non-AVC growth due to the faster ampoule translation rate, but AVC growth resulted in a value of K_{eff} closer to K_o. In order to explain this effect using the BPS equation, the introduction of vibrations must have decreased the thickness of the diffusional boundary layer (δ) as K_o and D are constants. A decreased boundary layer thickness upon application of AVC was expected based on the mathematical modeling discussed previously.

Dopant segregation can be an important aspect to the crystal growth of many systems. The data from this model system, using Ag-doped sodium nitrate, have shown that AVC allows for faster growth rates, can improve radial composition uniformity by controlling the interface shape, and reduces the diffusional boundary layer thickness causing effective segregation coefficients closer to that of the equilibium values.

4.3.2 CVS

Sodium nitrate was chosen as a model low temperature growth system to study the influence of CVS on the actual growth process. The $NaNO_3$ experiments were used to determine the effects of CVS induced flows on the interface shape and position, growth rate stability, and temperature gradients in the melt system.

4.3.2.a Static (Non-Growth) Experiments

The original paper on CVS [13] contained a short section describing a meltback effect in $CsCdCl_3$, in which the solid-liquid interface moved downward in the crucible with increasing frequency. The interface was found to move as much as 1 cm under a vibrational frequency of ~5 Hz. Due to the importance of such a strong meltback effect on crystal growth and its implications regarding heat and mass transport in the system, this effect was studied more thouroughly in this program using the $NaNO_3$ system.

A series of experiments were designed to measure the effect of CVS generated flows on the solid-liquid interface position under non-growth conditions. These were performed using the 1st generation transparent furnace under a 20°C/cm furnace gradient. Vibrational frequency was set to a specific value, allowed to stabilize for ~1hr, then measurements were taken. Interface position was monitored using a CCD camera connected to a video monitor. Temperature variations were monitored using two thermocouples: one near the melt and one near the solid as seen in figure 43.

Figure 43 shows the result of an interface position versus frequency experiment for an interface initially 23 mm from the melt surface. The nature of the CVS process (the fact that the crucible must move in a circle) dictates that the crucible cannot start in the exact center of the furnace. Therefore, when vibrations of any frequency are used, the crucible begins moving. This alters the thermal profile and thus the interface position. The initial 5 mm drop from rest position seen in figure 43 is due to this effect. At 5.8 Hz, the interface position becomes strongly dependent on the vibrational frequency. Such effects might be expected if strong CVS flows reach the solid-liquid interface. The flows would bring hot liquid from the top of the melt down to the growth interface raising the temperature at the solid-liquid interface and causing the solid to melt. Because the thermocouples are at a fixed position, a temperature rise would be expected in the solid as the solid-liquid interface moves closer to that point. A slight decrease in temperature of the liquid is possible due to the latent heat needed to melt the solid. The green line in figure 43 shows the

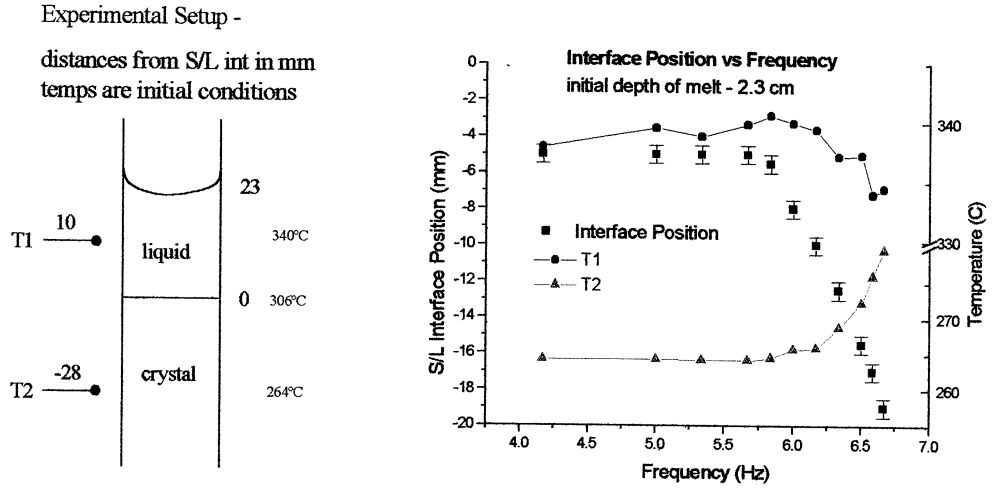

Figure 43. Plot of interface position and temerature versus vibrational frequency (right) and experimental setup (left)

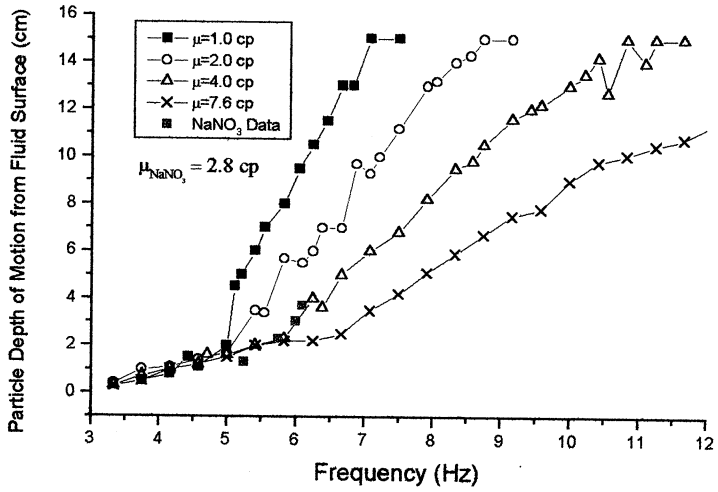

Figure 44. Plot showing correlation between interface motion and depth of flows

corresponding temperature rise in the solid with increasing frequency and the red line shows a slight temperature drop in the melt.

Similar trends for interface position and temperature were found in experiments performed on melt depths of 13 mm, 30.5 mm, and 37 mm. In figure 44, the interface position data taken from all four of the melt depths was plotted along with the depth of motion data generated in the water/glycerin experiments to determine if any correlation between interface position and depth of fluid flow existed. The $NaNO_3$ data (green dots) was taken at the frequencies at which interface position became stongly dependent on frequency for each of the melt depths. The $NaNO_3$ data is shifted slightly to the right of where it should fall. This can be explained by the fact that the $NaNO_3$ crucible diameter was slightly smaller than the ampoule used to generate the depth of motion data (1.8 cm versus 2.2 cm). Water/glycerin experiments have shown that smaller diameter crucibles require higher frequencies for the same depth of motion. Even with the slight shift, figure 44 makes a strong case for a correlation between fluid flow reaching the interface and the interface position dependence on frequency.

Figure 45 shows a typical plot of the relationship between interface position and time. Steady state takes approximately 30 minutes at 6.67 Hz for an initial melt depth of 2.3 cm. In comparision, steady state particle motion for the water/glycerin experiments was achieved in only 1-2 minutes. Such data suggest that mass transport takes place much more rapidly than thermal transport in this type of system.

Changes in the temperatures in the liquid and solid are also plotted versus time in figure 45. At first the temperature in the liquid rapidly falls as latent heat (110 kcal/mol [25]) is absorbed from the liquid by the solid in order to cause melting. After about 10 minutes, the liquid begins to regain some of its heat until reaching a steady state value in about 45 minutes. The temperature in the solid increases as the meltback occurs and the solid-liquid interface gets closer to the thermocouple.

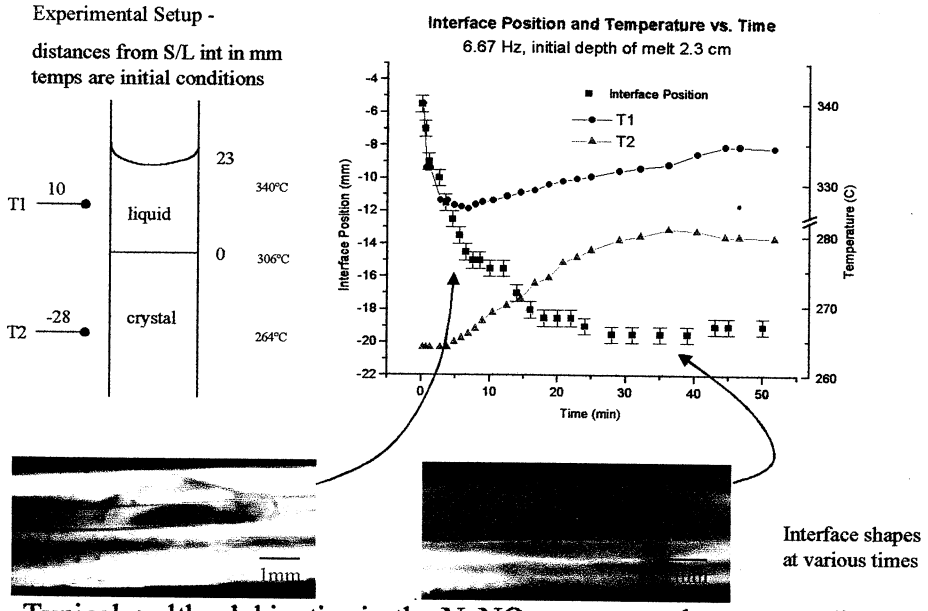

Figure 45. Typical meltback kinetics in the $NaNO_3$ system and corresponding interface sha

When the interface moves by only a couple of millimeters, its shape typically does not change. However, when the interface moves a centimeter or more due to fluid motion, the interface shape has been found to change during meltback. In the initial, most rapid portion of the meltback seen in figure 45, the solid-liquid interface becomes concave near the sides of the crucible, but forms a conical peak in the center. This shape is consistent with expected flow behavior of CVS: bringing hot fluid from the top down the sides of the crucible and then pushing the melt back to the surface in the middle of the crucible. After ~12 minutes, the interface regains the flat but slightly concave shape that was present before the vibrations were initiated.

4.3.2.b $NaNO_3$ Growth Experiment

After learning how CVS flows affect the $NaNO_3$ melt system in a non-growth mode (i.e. no crucible translation), experiments were undertaken to evaluate its effect on $NaNO_3$ under actual growth conditions. It has previously been shown that as frequency is changed, the magnitude and depth of the flows change. Growth experiments were undertaken to determine the effect of CVS flows on growth as the aspect ratio changes during Bridgman growth (the solidifying interface approaches the fluid surface). Interface position was monitored during growth using a CCD camera attached to a video monitor, and temperatures were monitored with thermocouples as in the previous experiments. The initial melt depth was set at 6 cm, the furnace motion rate at 10 mm/h, and the furnace gradient at 20°C/cm. Experiments were performed first without vibrations and then with three different vibrational frequencies set to give flows through melt depths of 6 cm, 4 cm, and 2 cm (6.3 Hz, 6.0 Hz, & 5.5 Hz respectively). These flow depths were based on the viscosity of $NaNO_3$ (2.8 cp) and the depth of motion curve (figure 44). Figure 46a shows a schematic of the flow depth expected from given vibrational frequencies (red - 6.3 Hz, blue - 6.0 Hz, light blue - 5.5 Hz) with the crystal growing into the expected flows as growth proceeds. It is important

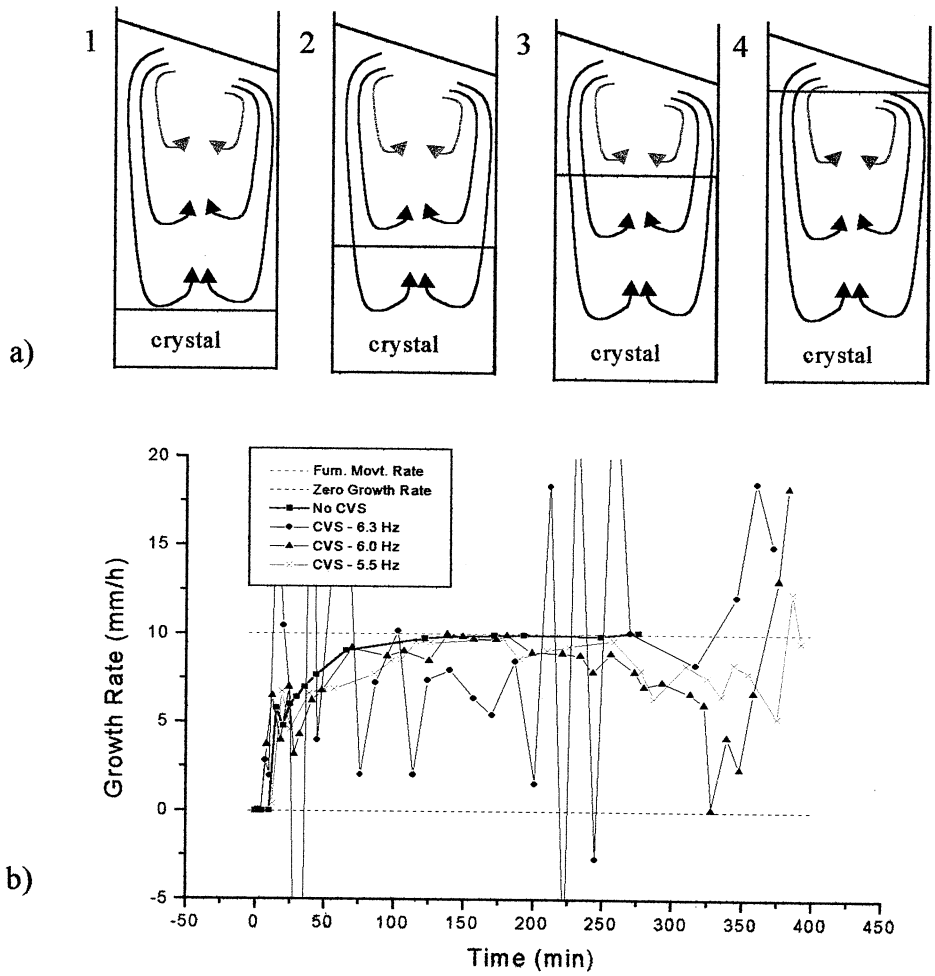

Figure 46. Growth rate experiments with and without CVS. 46a shows flows produced due to frequency settings. Colors of flows in 46a correspond to colors of the growth rate curves in 46b (i.e. light blue curve corresponds to a frequency setting of 5.5 Hz for both 46a & 46b). 46a also shows the crystal growing with time (1 being near the start of growth and 4 being near the end). Each of the frequency settings are associated with a velocity profile with the fastest flows present near the surface and zero flow at the point where the arrows reverse direction in 46a. As the crystal grows into the expected flows (46a), flows are disrupted by the solid-liquid interface and the interface encounters stronger flows as it approaches the fluid surface.

to remember that a velocity gradient is produced by this technique with the highest velocity near the surface and zero velocity where the flow depth ends.

In the experiment without vibrations (figure 46b - black curve), the growth rate initially lagged behind the rate at which the furnace was moving (green curve) but eventually reached a steady state at the furnace movement rate. This type of behavior in Bridgman growth is well known and has been attributed to the thermal coupling between the furnace and charge and latent heat generation at the interface [27]. At 6.3 Hz (figure 46b - red curve), the growth rate behaved erratically, switching from very fast growth to melting back (negative growth rate). Erratic growth rate behavior such as this is highly undesirable in crystal growth and can cause many problems.

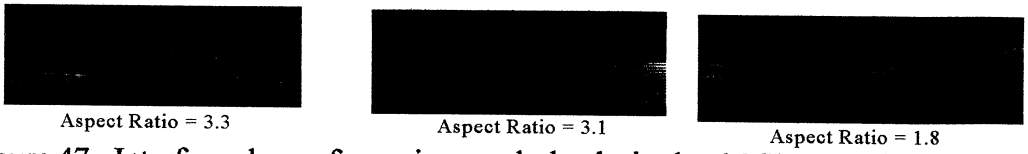

Figure 47. Interface shapes for various melt depths in the 6.3 Hz growth experiment as growth proceeds. Aspect ratio refers to the liquid height / crucible diameter

The intermediate frequencies (6.0 and 5.5 Hz) produced more subdued growth rate variations. For both of these frequencies, growth started out much the same as in the case without vibrations, i.e. the growth rate lagged behind the furnace movement rate and eventually reached the same rate. However, both growth rates began to slow toward the end of the growth experiment as moving fluid reached the growth interface. Neither frequency produced a melting effect (negative growth rate) and rapid growth (faster than the furnace traslation rate) was only seen during the last 20 minutes of growth. The growth rate did begin to deviate significantly from the furnace translation rate when strong fluid flows began to reach the growth interface. Not surprisingly, the stronger flows (6.0 Hz) interacted with the growth interface earlier and created larger deviations from the desired growth rate when compared to the weaker flows (5.5 Hz).

In addition to growth rate fluctuations, all three of the applied frequencies produced interface shape changes toward the end of the growth. Interface shapes as a function of aspect ratio for the 6.3 Hz experiment can be seen in figure 47. Interfaces started out flat with a slightly concave curvature near the crucible walls. This shape is consistent with the previous, non-growth experiments. As growth progressed, the strong flows began interacting more with the growth interface. As a result of the interaction, the interface became more concave and sloped. Near the end of growth the interface had a distinctive s-shape. These s-haped interfaces were only seen during crystal growth, suggesting that the shape was produced as a result of kinetic processes such as the removal of latent heat. Interface shape changes were quite pronounced, and occured earlier in the growth process (at larger aspect ratios) at the higher frequencies. All three frequencies showed changes in interface shape toward the end of the growth run (aspect ratio < 1).

Previous CVS growth experiments did not report unusual growth rate behavior or interface shapes [13, 15, 16]. Because growth conditions such as furnace gradients and furnace movement rates affect the growth rate behavior and/or interface shapes, the growth conditions were varied in order to to determine their influence on the $NaNO_3$ system.

4.3.2.c Furnace Gradient Effects

Three furnace gradients were examined (8.5, 20, and 26 °C/cm) in order to determine their effect on interface shape and motion. The experiment was performed at a vibrational frequency of 6.25 Hz and an initial melt depth of 2.5 cm. Figure 48 shows a plot of interface position versus time from the start of vibrations. The plot shows that the steeper furnace gradients shifted less under the influence of identical CVS flows (~6 mm for 26 °C/cm

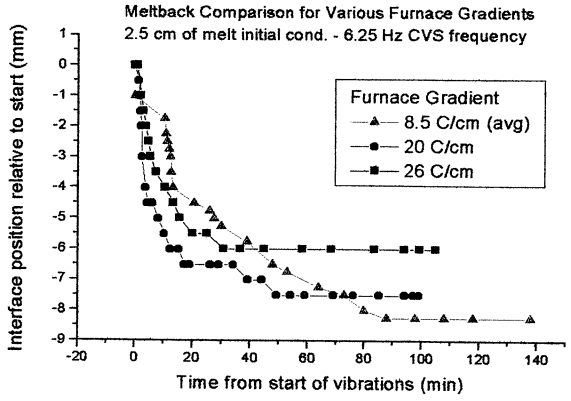

Figure 48. Interface motion for different gradients under CVS flow

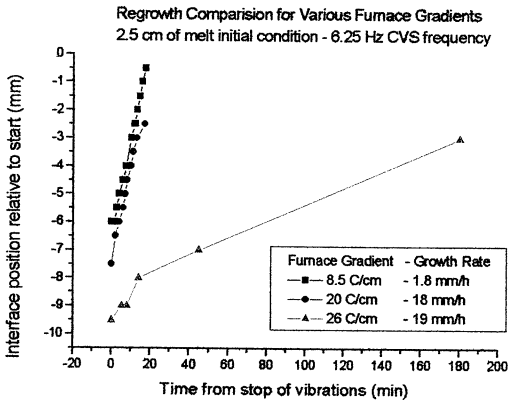

Figure 49. Interface motion for different gradients after CVS flow is removed

versus ~8.5 mm for 8.5 °C/cm). Interfaces in steeper gradients also acheived their steady state position faster than the shallower gradients (~30 min for 26 °C/cm versus ~90 min for 8.5 °C/cm). Note that the 8.5 °C/cm gradient produced a sloped interface and that an average position was recorded. This data suggests that steeper furnace gradients might suppress the rapid meltback seen in previous growth experiments by not allowing the solid-liquid interface to fluctuate as much under CVS flows.

As shown in figure 49, the interfaces began to move back toward their original positions (before vibrations were applied) when the vibrations were stopped. Growth rates were calculated based on the slope of the curves in figure 49. The interfaces moved faster in steeper gradients once the vibrations were removed: the 8.5 °C/cm gradient had a regrowth rate of 1.8 mm/h, the 20 °C/cm gradient had a regrowth rate of 18 mm/h, and the 26 °C/cm gradient had a regrowth rate of 19 mm/h. None of the interfaces returned to the exact position they held prior to introducing CVS. This is possibly due to a slight position difference of the crucible relative to the furnace once crucible motion stopped. Rapid regrowth, such as that seen in the steeper gradients, should be avoided in order to prevent the formation of striations and other defects.

The 8.5 °C/cm gradient produced a sloped interface (flat but at a different position from one side of the crucible to the other) without vibrations, while the other two gradients produced flat interfaces normal to the growth axis. In shallow gradients, the slope of the interface increased and the shape became concave once the fluid flow started. The steady state concave shape is shown in figure 50. The difference in height from one side of the

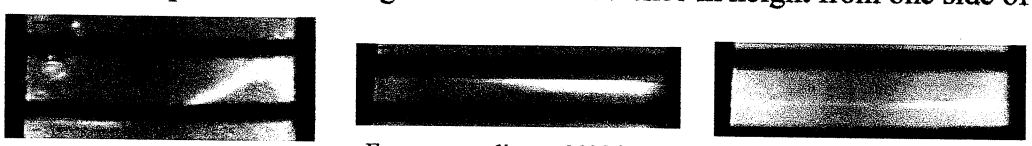

Furnace gradient - 8.5°C/cm
90 min after vibrations

Furnace gradient - 20°C/cm
69 min after vibrations

Furnace gradient - 26°C/cm
100 min after vibrations

Figure 50. Interface shapes under different furnace gradients at steady state position during flows

crucible to the other was ~ 4mm without CVS, while the steady state interface shape had a strong concavity and a height difference of ~ 8 mm. The two steeper gradients stayed flat both before and during CVS.

In summary, the shallower temperature gradient had slow regrowth rates and also created an undesirable interface shape. Steeper gradients promoted flat interfaces and melted back less under CVS generated flows, making them more likely to create a more stable growth environment. Regrowth rates were rapid under steep gradients, and therefore must be taken into consideration when designing experiments that involve changing fluid velocities near the interface.

4.3.2.d Effect of Furnace Translation on Interface Stability

We believe that the instabilities in the growth rate under strong flows, as shown in figure 46, are due to unstable CVS flows resulting in temperature fluctuations in the melt. A temperature increase at the growth interface will slow the growth rate or in extreme cases cause meltback. The more damaging aspect of unstable flows occur when the temperature drops at the growth interface, causing rapid solidification. At a slower growth rate, latent heat generation will be slower. By introducing heat into the melt at a slower rate, it was thought that large temperature fluctuations could be avoided. The effect of the furnace motion rate on growth rate was measured in a similar experiment to that plotted in figure 46. In this experiment, the vibrational frequency was kept at 6.3 Hz (the red curve from figure 46) but the furnace movement rate was lowered to 2.3 mm/h.

Figure 51 shows a comparison between growth rate fluctuations with a slow and fast furnace translation rate under otherwise identical growth conditions. In order to make the comparison easier, growth rates were normalized with respect to the furnace translation rate, and time was normalized with respect to the total growth time. No vibrations were used to generate the black curve. It is shown as a control to demonstrate normal growth

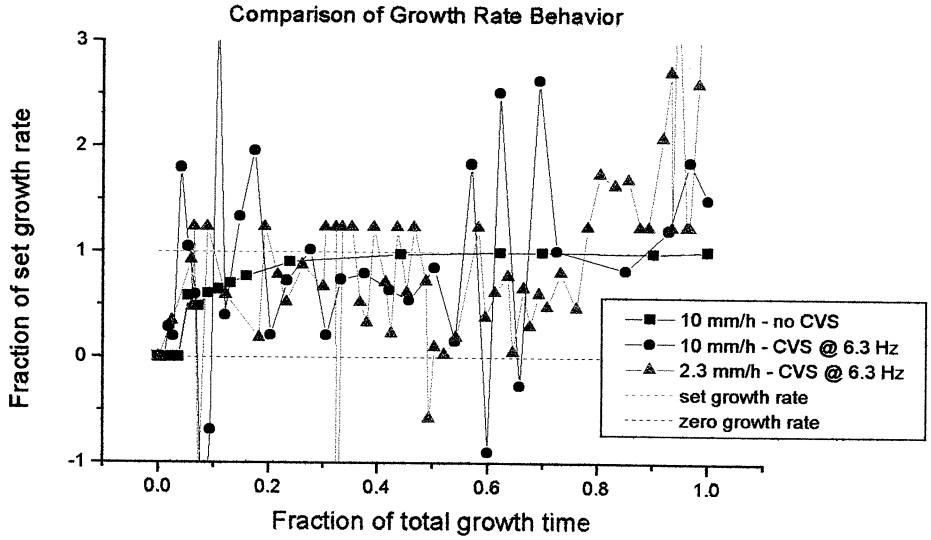

Figure 51. Comparison of growth rate flucuations for two different furnace translation rates under CVS flows

behavior. The faster furnace translation rate (red curve) shows growth rates which greatly exceed the furnace translation rate along with growth rates much slower than the translation rate, including some meltback. While the slower furnace translation rate (green curve) contains growth rates slower than the furnace translation rate and some meltback, no rapid growth was observed until the end of the growth run. The fast growth seen at the end of both CVS growth runs is due to end effects in the system and could possibly be avoided by reducing the frequency as the fluid aspect ratio decreases.

In summary, slower furnace translation rates reduced the magnitude of the fluctuations of growth and dissolution rates, especially growth rate fluctuations. It is therefore more desirable to use slow translation rates for growth under CVS conditions.

4.4 High Temperature Melt Experiments

4.4.1 AVC

4.4.1.a TeO_2

Paratellurite (TeO_2) was the first high temperature material chosen for study using the AVC system.

Paratellurite was produced by low temperature oxidation of powdered Te (99.9999%) in dry oxygen. A schematic of the synthesis system is shown in figure 52. Charge synthesis required two steps. First, powdered Te was oxidized at 430°C which is lower than the Te melting point (449°C). The result of this step was Te grains covered with an oxide film. The second step involved heating the system to 600°C and increasing oxygen pressure to

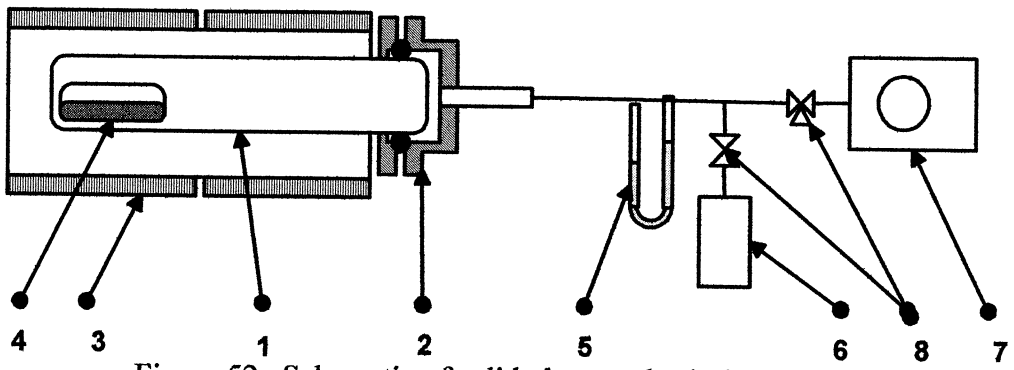

Figure 52. Schematic of solid phase sythesis for TeO_2

1. quartz reactor
2. flange with seal assmebly
3. two zone resistive furnace
4. ampoule with elemental Te
5. manometer
6. oxygen reservoir
7. vacuum pump
8. vacuum valve

600 torr in order to promote oxygen diffusion. The stoiciometry of the charge could be varied by changing the oxygen pressure. The final product was white grains of 5-10 μm.

Paratellurite melts are highly reactive with quartz. In order to provide a coating that was non-reactive with TeO_2, Pt was thermally sputtered onto the inside surface of the quartz ampoule under a high vacuum. Paratellurite growth was attempted several times in the Pt coated quartz ampoules without vibrations. However, we failed to get a single crystal because the melt reacted with the quartz. It was thought that small holes or inhomogeneities were present in the Pt lining. Several attempts were made to improve the coating, but none were successful.

4.4.1.b PbTe

Because the experiments with paratellurite had not been successful, PbTe was picked as an alternative high temperature compound because it is inert toward quartz. Lead telluride melts at 924°C and was synthesized by directly melting Te and Pb refined from the oxide.

Lead telluride is reactive in air, so it had to be grown either under a vacuum or an inert atmosphere. Single crystals were successfully grown with and without vibrations using a growth rate of 3 mm/h and an argon atmosphere in the first generation high-temperature AVC system. At this point, we realized that modifications to the system were needed and the second generation furnace was designed and fabricated.

The second generation furnace allowed for growth under a vacuum, which was used to grow crystals without vibrations. However, many technical difficulties had to be overcome to use AVC. AVC motion caused the PbTe melt to vaporize much more than under non-vibrating conditions. If the argon pressure was not high enough in the system, then the PbTe would condense on the vibrating rod, causing the system to lock up.

Table 2 lists the atmoshpere conditions and measured properties of the nine successful PbTe growth runs. Numbers 1-5 were grown without vibrations and 6-9 used AVC vibrations with a frequency of 50 Hz and an amplitude of 100 μm. Figure 53 shows a picture of one of the AVC grown PbTe crystals.

Crystals grown with and without AVC had similar carrier concentrations, carrier mobililities, and dislocation densities. It is possible that the crystal quality can be improved if the vibrational parameters are optimized to the PbTe system, but we were not able to accomplish this over the time period of the report.

Table 2. PbTe Growth Results

Run	Conductivity type of the raw substance	Gas atmosphere	Crystal properties			
			Conductivity type	Carrie concentration < p(n) cm^{-3}	Carrie mobility μ, $cm^2V^{-1}s^{-1}$	Dislocation density, cm^{-2}
1	*p*	Vacuum (ampoule)	*p*	$2,0*10^{18}$	560	$2,3*10^{6}$
2	*n*	Vacuum	*n*	$1,2*10^{18}$	340	$3,5*10^{5}$
3	*p*	Vacuum	*p*	$4,1*10^{18}$	540	$3,4*10^{5}$
4	*p*	Vacuum	*p*	$3,9*10^{18}$	460	$3,3*10^{5}$
5	*n*	70 torr Ar	*n*	$4,9*10^{18}$	620	$3,0*10^{5}$
6*	*p*	700 torr Ar	*p*	$5,0*10^{18}$	250	$8,0*10^{5}$
7+	*n*	200 torr Ar	*p*	$1,5*10^{17}$	320	
8	*p*	300 torr Ar	*p*	$5,7*10^{18}$	390	$2,5*10^{5}$
9	*p*	400 torr Ar	*p*	$2,7*10^{18}$	550	$1,3*10^{5}$

*- growth in 1st generation furnace

+ - crystal was oxidized due to ampoule crash

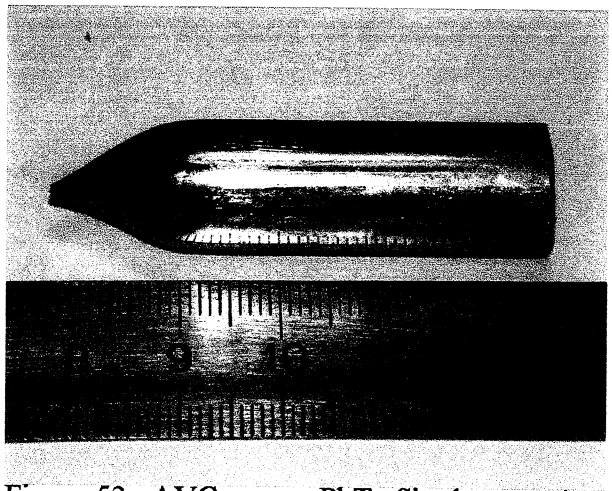

Figure 53. AVC-grown PbTe Single crystal

4.4.2 CVS (PMNT)

PMNT ([1-x] $PbMg_{1/3}Nb_{2/3}O_3$ - x $PbTiO_3$) is one of a number of new and important relaxor ferroelectric materials having very high dielectric constants and electromechanical coupling coefficients. It is a solid solution between $PbMg_{1/3}Nb_{2/3}O_3$ and $PbTiO_3$ and as a result most compositions are incongruently melting. The properties of PMNT are highly dependent upon Ti composition particularly near the morphotropic phase boundary (which seperates the rhombohedral and tetragonal phases) where the material exhibits its

best properties. The current preferred method to grow single crystals of this material is the Bridgman technique [26]. However, composition profiles of large (> 1 inch) diameter crystals show significant Ti variations along the growth direction. These variations follow the classic relationship for unidirectional solidification in a system where the melt is completely mixed via buoyancy driven convection. In this case, the composition continuously changes with distance. Compositional profiles containing small transients at the beginning and end of the boule but uniform along the bulk of the crystal are acheived only in convectionless melts (i.e. under diffusion controlled growth conditions). To get a boule of mostly uniform composition, it is therefore desirable to reduce or eliminate convection. Toward the end of this study we explored the possibility of using CVS flows to damp natural convection in order to produce more compositionally uniform crystals.

One experiment was designed to test the effect of CVS flows on the compositional uniformity of PMNT crystals. Based on data obtained during the course of this program, we understand that an important issue to be considered was the strong dependence flow velocity and depth on the height of the melt. Since our goal was only to dampen flows, not induce vigorous melt mixing, we needed to decrease the frequency continuously during growth because the melt height decreases as the crystal grows. The continuously decreasing frequency would also help to avoid the growth instabilities seen in the $NaNO_3$ system under continuous, strong flows. Because we did not have the capability at the time to ramp down the frequency electronically, the frequency changes were made manually in small increments during the growth run.

As mentioned in the experimental procedure section, the Pt crucible diameter was 1.8 cm and the growth temperature of this composition was ~1300°C. The furnace gradient at the growth temperature was set to 20°C/cm. The initial melt depth (seed to melt surface) in the experimental setup was calculated to be 6.9 cm. As previously seen, the depth of motion in CVS is heavily dependent on viscosity (figure 34). Because a literature value for the viscosity of PMNT is not known, the viscosity was estimated to be similar to that of $NaNO_3$ because both are oxide melts. Using figure 34, it was estimated that a frequency of 7.2 Hz would be needed to get the CVS induced flows to reach the inital growth interface.

Figure 34 shows that at frequencies >5Hz, the depth of motion curves have relatively constant slopes. Using a growth rate of 0.8 mm/h (the growth rate commonly used by our lab to grow this material) and the slope calculated for a 3 cp fluid (from figure 25), the required rate of frequency reduction was calculated to be 1.75 RPM/h (0.029 Hz/h).

The experiment, while carefully setup, was only partially successful. First, the Pt crucible leaked (an all too common occurance in the Pt-PMNT system) somewhere near the beginning of the growth run and about 2 cm of melt height (36% of the charge) was lost. This was a greater leakage then in normal Bridgman growth and may have been exacerbated by the flowing melt on the walls of the Pt crucible. Because of the lowered aspect ratio, more vigorous mixing was created than intended. Despite the leaking, a rather large boule still resulted. Figure 54 shows a thin axial cross-section of the resulting boule, along with the manual frequency ramp, and the Ti composition profile.

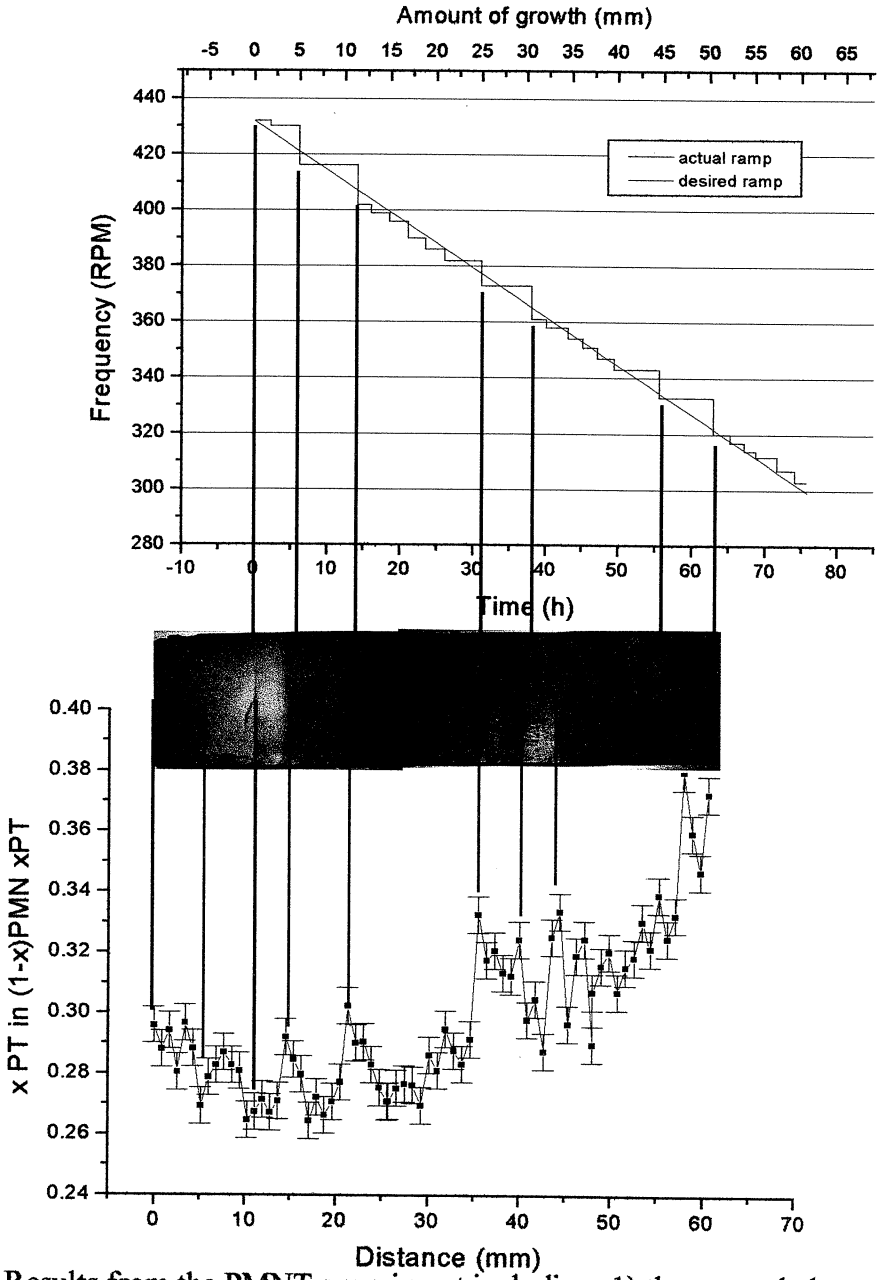

Figure 54. Results from the PMNT experiment including: 1) the manual changes in frequency with time, 2) a photograph of a thin cross section along the growth axis and 3) the corresponding Ti concentration

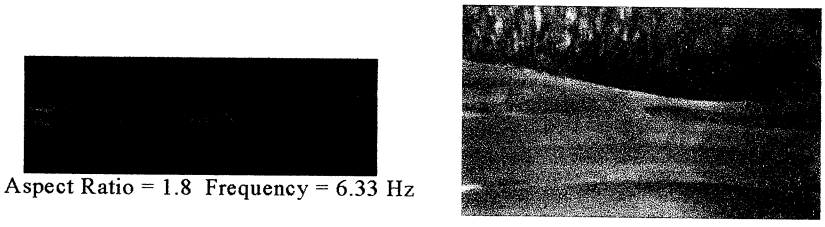

Aspect Ratio = 1.8 Frequency = 6.33 Hz

Aspect ratio - 1.9 Frequency - 6.37 Hz

Figure 55. Comparison of $NaNO_3$ (left) and PMNT (right) interface shapes under similar conditions

The boule showed a number of interesting features not previously seen in PMNT material. The most dominant features were striations and inclusions. The most dominant striations can be correlated to the largest of the manual frequency changes made during the growth run. The effect of CVS generated flows on the heat transfer in the system was larger than we expected. Therefore a small frequency change produced a very large thermal change in the system causing the growth rate to increase sharply, trapping low k material segregated at the interface and thereby creating a striation.

Also shown in figure 54 is the Ti concentration profile. Overall, it increases continuously as in the non-stirred melts. This is not surprising as there was much more vigorous mixing than intended due to the reduction of the melt height from leaking. This experiment therefore did not acheive its goal of making the PMNT boule more uniform. Larger compositional variations (peaking of Ti concentration) also occurred in this boule relative to non-stirred melts. The peaking is consistent with the striation position and with the low Ti segregation coefficent. During steady state growth, the Ti concentration normally builds up at the interface to a value dependent on the details of the phase diagram. When rapid growth occurs, the high Ti concentration is trapped into the growing crystal.

The striations created by manual frequency control revealed the shape of the solid-liquid interface along the growing crystal. The interface shape changed from a convex interface at the bottom of the boule to an s-shaped interface near the top, much like the ones seen in $NaNO_3$ (figure 47). A comparison of the interface shape for PMNT (AR =1.9) can be seen next to a similar interface generated in $NaNO_3$ (AR=1.8) in figure 55.

The PMNT appears to have behaved in a remarkably similar manner to the $NaNO_3$ under CVS flow conditions. Future experiments that control the leaking problem and create a smoother frequency ramp should produce more desirable results.

Because real growth systems such as PMNT appear to behave similar to our $NaNO_3$ model system, experiments to correct problems such as the growth rate fluctuations observed under CVS flows can be beneficial. The $NaNO_3$ experiments are much faster and cheaper to perform than PMNT experiments, so that knowing how the $NaNO_3$ system responds to similar parameter changes should save both time and money in the design of future PMNT experiments.

5.0 Conclusions

Over the course of this project, much knowledge has been gained in understanding how low frequency vibrations introduced through the AVC and CVS methods affect fluid flow and growth behavior in crystal melt environments. A series of model systems were used to investigate the AVC and CVS systems including: mathematical models, non-crystallizing systems, and low temperature transparent crystallizing systems. Both systems produce complicated flows that are governed by multiple parameters. Knowledge gained through the modeling was applied toward the growth of technologically important materials. Although our understanding of the important issues involved in using these techniques has improved, further work will be required in order to easily and effectively apply AVC or CVS to solve crystal growth problems. The main items of progress over this report period are as follows:

Equipment fabrication and systems studied:

- Equipment to study fluid flow for AVC/CVS with water/glycerin was designed and fabricated.
- Transparent furnaces to study AVC/CVS effects on sodium nitrate were designed and fabricated.
- CVS was used to grow a crystal of PMNT from a high temperature melt.
- Two high temperature/controlled atmosphere furnaces were designed/fabricated for AVC.
- AVC was used to grow several crystals of PbTe from a high temperature melt.
- Software to analyze fluid flows (velocities and flow patterns) was developed and used in flow analysis.
- Flow visualization for CVS/AVC was achieved for water/glycerin systems.

Understanding of CVS fluid flow:

- A combination of dye and particle tracer experiments were used to characterize fluid flow under CVS vibrations under various operating conditions.
- Specific vibrational, geometrical, and fluid parameters were established as important.
- The effect of changing these established parameters on different fluid flow parameters (mix time, wave height, resonance freq, fluid velocity, flow patterns, depth of flows from surface) was measured.
- CVS flows originate at the free surface of the melt.
- A velocity gradient is present in CVS generated flows with the highest average velocity near the surface and a zero velocity lower in the melt. The position of the zero point depends on the energy provided to the system, fluid properties, and crucible geometry.

- Wave height collapse was found to be correlated to an increase in mixing time. In small diameter crucibles (3.2 cm or less) waves did not collapse.
- Depth of motion was found to be very sensitive to the vibrational frequency, fluid viscosity., and crucible diameter.
- CVS generated flows can be made to damp or reverse flows generated through a propeller driven mixer.
- CVS generated flows do not exist in a crucible with a fully clamped surface under gradients produced in our laboratory environment.
- Clamping the surface with a small bubble of air present will allow CVS to generate flows.
- Based on the data collected, inertial forces seem to be the driving force for fluid motion. The wave height is a measure of the energy input.
- An equation for relating upward and downward flow volumes to upward and downward average velocities was developed using a mass balance for CVS.

Effect of CVS flows on melt systems:

- CVS fluid flow has a strong effect on interface position in the sodium nitrate system. This effect is a strong function of vibrational frequency once strong flows reach the interface.
- Important time scales in water/glycerin and sodium nitrate are not the same. Mixing times in water/glycerin take place in seconds. Interface motion in sodium nitrate due to convection related heat transfer takes up to an hour to stabilize.
- Interface motion in the sodium nitrate system due to CVS flows can be predicted using the depth of motion curves generated with the water/glycerin system.
- When strong flows reach the growth interface while growing using CVS, growth rate fluctuations result.
- During CVS growth, interface shape changes occur under strong flows. (goes from flat to s-shaped)
- Using a steeper furnace gradient will cause the interface to shift less under CVS flows in a non-growth environment.
- Slower furnace motion rates cause less severe fluctuations in growth rate under strong CVS flows.
- Interface shapes observed in sodium nitrate also appear in PMNT under similar flow conditions.
- PMNT striations correlate to large changes in frequency. Future experiments must use a more continuous frequency change.

Understanding of AVC fluid flow:

- Finite element models were used to solve AVC flow problems under various operating conditions.
- AVC flows predicted from mathematical modeling matched with those observed in the water/glycerin and sodium nitrate system.
- Mathematical modeling in AVC showed that by changing the frequency of vibration, flow intensity and direction can be manipulated as well as the thermal profile of the system. Simulations found this to be true in both terrestrial and microgravity environments.
- AVC flight experiment was performed on Mir using a water/glycerin system.
- Flows produced through AVC were found to be stronger and more sensitive to the vibrational reynold's number in a micro-gravity environment than in a terrestrial one.

Effect of AVC flows on melt systems:

- In AVC, by adjusting the vibrational parameters, the interface shape in the sodium nitrate system could be altered. Convex, concave, and flat interfaces could be achieved with the appropriate system settings.
- In AVC, dislocation density in sodium nitrate decreased when the vibrational amplitude (flow rate) was increased.
- In AVC, radial concentration profiles can be altered by changing the vibrational parameters. Radial profiles are a function of the interface shape (as expected).
- In AVC, segregation coefficients for Ag dopants become closer to equilibrium values under vibrational flow. This effect can be explained with a decrease in diffusional boundary layer thickness which is expected from mathematical models.

In summary, a greater understanding was gained concerning the parameters necessary to control fluid flow using the CVS and AVC systems as a result of this project. Knowledge was also gained concerning the effect of forced convection produced through these techniques on crystal melt systems. AVC was found to have a larger effect than CVS on controlling growth interface shape. CVS does not require vibrators to be introduced into the melt, making it easier to use for sealed systems than AVC. Both techniques were found to produce controllable convection and have the potential to benefit the crystal growth community.

6.0 References

1. B. Langenecker, W.H. Frandsen. "The Influence of Sound Waves on the Growth of Zinc Crystals" Phil. Mag. 7 (1962).
2. A.F. Witt, H.C. Gatos. "Determination of Microscopic Rates of Growth in Single Crystals" J. Electrochem. Soc. 114 (1967).
3. G.M. Ikonnikova, A.P. Izergin. "Effect of Low Frequency Vibrations in the Melt on the Shapes and and Properties of KCl Crystals" Growth of Crystals, Ed. N.N. Sheftal (Consultants Bureau, New York), 68 (1968) 82.
4. A.S. Borshchevskii, D.N. Tretjakov. "On the Influence of Vibrations on the Crystallization of some Semiconductors" Kristall and Technik 34 (1968) 69.
5. G.V. Nikitina, V.N. Romanenko, V.M. Tuchkevich. "Kristallizatsia i fazovye perekhody (Crystallization and Phase Transformations)" collection of papers, Minsk, USSR, 1962, page 379 (in Russian). (Publishing House of the Academy of Sciences of USSR)
6. A.N. Krigintsev, E.G. Avvakumov. "A Method of Stirring the Melt in Controlled Crystallization" Svt. Physics-Crystallography, 10 (1965) 449.
7. R.S. Feigelson. Private communication.
8. J.I.D. Alexander. "Low Gravity Experiment Sensitivity to Residual Acceleration." A review. Microgravity Science and Technology, III, 1990 p. 52.
9. D. Schwabe, A. Scharmann. J. Crystal Growth, 46 (1979) 125.
10. S.-E. Park, T.R. Shrout. J. Appl. Phys., 82 (1997) 1804.
11. S.L. Swartz, T.R. Shrout. Mater. Res. Bull., 17 (1982) 1245.
12. O.A. Bushmakin, N.A. Verezub, E.V. Zharikov, A.Z. Myal'dun, A.I. Prostomolotov. "Fluid flow in a cylindrical vessel in the presence of an axially vibrating disk." Fluid Dynamics, 32 (1997) 366.
13. W.-S. Liu, M.F. Wolf, D. Elwell, R.S. Feigelson. "Low frequency Vibrational Stirring: A New Method for Rapidly Mixing Solutions and Melts During Crystal Growth." J. Crystal Growth 82 (1987) 589.
14. A.I. Fedoseyev, D. Alexander. J. Crystal Growth, 211 (2000) 34.
15. Y.-C. Lu, J.-J. Shiau, R.S. Feigelson, R.K. Route. "Effect of Vibrational Stirring on the Quality of Bridgman Growth of CdTe." J. Crystal Growth 102 (1990) 807.
16. R.C. DeMattei, R.S. Feigelson. "The effect of forced convection on the melt gradient and growth rate during the Bridgman and gradient freeze crystal growth of silver-doped lead bromide." J. Crystal Growth 128 (1993) 1062.
17. E.V. Zharikov, L.V. Prihod'ko, N.R. Storozhev. "Fluid flow formation resulting from forced vibration of a growing crystal." J. Crystal Growth 99 (1990) 910.

18. E.V. Zharikov, N.A. Verezub, A.Z. Myal'dun, A.Z. Prostomolotov. "Effects of low frequency vibrations on temperature fluctuations in the melt for growth by the Czochralski method." Crystallography Reports 41 (1996) 354.

19. N.A. Verezub, E.V. Zharikov, S.P. Kalitin, S.V. Lavrishchev, A.Z. Myal'dun, Yu.M. Papin, A.I. Prostomolotov, N.R. Storozhev. "Effect of controlled low-frequency vibrations on melt in growth of yttrium-scandium-gallium garnet single crystals." Crystallography Reports 41 (1996) 1056.

20. D. Schwabe, A. Schrmann, R. Preisser, R. Order. "Experimetns on surface tension driver flow in floating zone melting." J. Crystal Growth 43 (1978) 305.

21. V.D. Golyshev, M.A.Gonik., (1995) Terrestrial experimental research of new method features of large single crystal growth. In: Proc. Microgravity sci. and aplications session, Int. Aerospace Congr., Moscow, August 16-17,1994,Moscow, pp.167-171.

22. N.G.Bourago, A.I.Fedyushkin, V.I.Polezhaev, (1997) Modelling of unsteady submerged heating crystal growth in ground-based and microgravity environment. Physical sciences in microgravity. Proceedings of joint Xth European and VIth Russian Symposium on Physical sciences in microgravity. St. Peterburg, Russia, 15-21 June 1997 , vol. II, pp.170-173,.

23. http://uahtitan.uah.edu/alex/cvs_frontx5.html

24. A. Fedoseyev. Private correspondence.

25. D.R. Lide, ed. CRC Handbook of Chemistry and Physics, 71st ed. CRC Press, Inc., Boca Raton (1990)

26. S.-G. Lee, R.G. Monteiro, R.S. Feigelson, H.S. Lee, M. Lee, S.-E. Park. "Growth and Electrostrictive Properties of $PB(Mg_{1/3}Nb_{2/3})O_3$ Crystals" Appl. Phys. Lett. 74 (1999) 1030.

27. T.-W. Fu and W.R. Wilcox. "Rate Change Transients in Bridgman-Stockbarger Growth." J. Crystal Growth 51 (1981) 557.